JOURNAL OF GEOPHYSICAL RESEARCH, VOL. 94, NO. C6, PAGES 8243–8264, JUNE 15, 1989

Simulations of Radiocarbon in a Coarse-Resolution World Ocean Model 2. Distributions of Bomb-Produced Carbon 14

J. R. TOGGWEILER, K. DIXON, AND K. BRYAN

Geophysical Fluid Dynamics Laboratory, NOAA, Princeton University, Princeton, New Jersey

Part 1 of this study examined the ability of the Geophysical Fluid Dynamics Laboratory (GFDL) primitive equation ocean general circulation model to simulate the steady state distribution of naturally produced ^{14}C in the ocean prior to the nuclear bomb tests of the 1950s and early 1960s. In part 2 we begin with the steady state distributions of part 1 and subject the model to the pulse of elevated atmospheric ^{14}C concentrations observed since the 1950s. This study focuses on the processes and time scales which govern the transient distributions of bomb ^{14}C in the upper kilometer of the ocean. Model projections through 1990 are compared with observations compiled by the Geochemical Ocean Sections Study (GEOSECS) in 1972, 1974, and 1978; the Transient Tracers in the Ocean (TTO) expedition in 1981, and the French INDIGO expeditions in 1985–1987. In their analysis of the GEOSECS ^{14}C observations, Broecker et al. (1985) noted that much of the bomb ^{14}C which entered the ocean's equatorial belts prior to GEOSECS accumulated in the adjacent subtropical zones. Broecker et al. argued that this displacement of bomb ^{14}C inventories was caused by the wind-driven upwelling and surface divergence in the tropics combined with convergent flow and downwelling in the subtropics. Similar displacements were invoked to shift bomb ^{14}C from the Antarctic circumpolar region into the southern temperate zone. The GFDL model successfully reproduces the observed GEOSECS inventories, but then predicts a significantly different pattern of bomb ^{14}C uptake in the decade following GEOSECS. The post-GEOSECS buildup of bomb ^{14}C inventories is largely confined to the subthermocline layers of the North Atlantic, the lower thermocline of the southern hemisphere, and down to 2000 m in the circumpolar region. A great deal of attention is devoted to detailed comparisons between the model and the available radiocarbon data. A number of flaws in the model are highlighted by this analysis. The Subantarctic Mode Waters forming along the northern edge of the circumpolar current are identified as a very important process for carrying bomb ^{14}C into the thermoclines of the southern hemisphere. The model concentrates its mode water formation in a single sector of the circumpolar region and consequently fails to form its mode waters with the correct *T-S* properties. The model also moves bomb ^{14}C into the deep North Atlantic and deep circumpolar region much too slowly.

INTRODUCTION

In the last decade, three-dimensional models of the ocean circulation have become increasingly important tools for understanding how the ocean works. In the near future, ocean circulation models will be asked to predict how the ocean will respond to widely anticipated perturbations of the global environment. Given this important challenge, model practitioners must be able to gauge how well their models work and be able to demonstrate the quality of their models to a larger audience. One of the most powerful means of demonstrating model performance is the simulation of the ocean's uptake of transient tracers. In part 2 of this study we describe model simulations of the uptake of bomb-produced radiocarbon in the Geophysical Fluid Dynamics Laboratory (GFDL) world ocean model [*Bryan*, 1969].

Part 1 of this study [*Toggweiler et al.*, this issue] explored the ventilation of the deep ocean through simulations of the distribution of natural radiocarbon. With a few exceptions, the GFDL model successfully reproduced the large-scale features of the deep radiocarbon distribution. The model's realization of the ocean's deep currents and large-scale overturning would appear to be a reasonable representation of real ocean processes. We found much of the decay of ^{14}C in the model's deep layers to be balanced by the model's slow, parameterized mixing of atmospheric ^{14}C across the thermocline. Much of the success of the radiocarbon simulation in part 1 must be attributed to the tuning of parameterized vertical diffusion over years of experimentation with the model using water mass properties as diagnostics.

Part 2 focuses on the set of ventilation processes which have allowed the ^{14}C produced by nuclear weapons tests to penetrate the upper kilometer of the ocean. The time scales of interest are of the order of 10–30 years, in contrast to the hundred- to thousand-year time scales of part 1. Transient tracer experiments hold up for scrutiny a set of model ventilation processes which are mainly advective. These bomb ^{14}C experiments identify some unrealistic features in the model; some are known from previous studies and some are identified here for the first time. It should be obvious to the reader that significant improvements are needed before the model's predictions for the future can be accepted at face value. On the other hand, the model's simulations offer new insights and pose new questions regarding the penetration of transient tracers and fossil fuel CO_2 into the interior of the ocean. They offer some specific, three-dimensional direction for planning ocean surveys in the 1990s.

Broecker et al. [1985] (hereinafter referred to as BPOS) produced an analysis of the bomb ^{14}C distributions in the ocean as observed by the Geochemical Ocean Sections Study (GEOSECS) expeditions during the 1970s, roughly 10 years after the input of bomb ^{14}C began. BPOS determined the vertically integrated inventories of bomb ^{14}C at all of the GEOSECS stations by estimating the prebomb profiles of ^{14}C at each location and subtracting these concentrations from those observed. They also estimated how much ^{14}C entered the ocean at each station location, using the ob-

Paper number 89JC00387.

served time history of atmospheric ^{14}C and independent knowledge about gas exchange rates. By mapping the bomb ^{14}C inventories and comparing these with input maps, BPOS showed that large-scale displacements of bomb ^{14}C inventory had occurred which were caused by ocean circulation. BPOS viewed these displacements as a consequence of the large-scale patterns in the wind field, which produce divergence and upwelling in the equatorial and polar regions and convergence and downwelling in the subtropics.

In part 2 of this study, a more detailed and quantitative analysis is attempted using the GFDL model. We have run bomb ^{14}C through five experiments making incremental changes to the vertical diffusion parameter, the gas exchange formulation, and the degree of restoring to the observed temperature and salinity fields. The presentation of our results is split into two time periods. The first time period corresponds to the decade following the end of the bomb tests, up to the time of GEOSECS. We compare model results with the BPOS maps of bomb ^{14}C surface concentrations and water column inventories to illustrate how well the model performs. We have also integrated the model to 1990, extrapolating the slowly declining atmospheric ^{14}C concentration curve from the measured trend of the early 1980s. The model predicts that the parts of the ocean which accumulate bomb ^{14}C after GEOSECS are not the same as those which accumulated bomb ^{14}C during the first decade of the postbomb era. A rather different pattern of bomb ^{14}C uptake evolves as processes and pathways with longer time scales come into play.

There are two important precursor studies for part 2. *Sarmiento* [1983] performed a bomb tritium simulation in the North Atlantic using the GFDL model. Sarmiento found that the spreading of tritium in the model is dominated by advection and winter convection. The main deficiency identified by Sarmiento was inadequate tritium penetration into the deeper layers of the North Atlantic thermocline in the northwestern part of the subtropical gyre. *Maier-Reimer and Hasselmann* [1987] performed a radiocarbon simulation for the world ocean (discussed in part 1), and also included bomb-tritium in their model. Maier-Reimer and Hasselmann did not simulate bomb ^{14}C.

Bomb radiocarbon and bomb tritium offer rather different views of the ocean's ventilation. The input of bomb ^{14}C to the ocean is spatially quite uniform relative to the input of tritium, which is concentrated in high northern latitudes. The global homogeneity of atmospheric bomb ^{14}C concentrations allows one to study the very important ventilation processes in the southern hemisphere. In addition, the slow decline of atmospheric ^{14}C after the mid 1960s, relative to the precipitous decline in tritium input, allows slower ventilation processes to be tagged with the bomb ^{14}C label.

MODEL DESCRIPTION

Summary of the Model

The ocean model has been extensively described in part 1, so the description given here will be brief. The model is built on a 4.5° latitude by 3.75° longitude grid with 12 vertical levels. It has coarsely resolved continental boundaries and bottom topography. Midpoint and interface depths of the model layers are given in Table 2 of part 1. The model is forced at the surface by observed, annually averaged temperatures, salinities, and wind stresses. There are no chemical transformations or transport of ^{14}C by biological processes. After a steady state is reached for the prebomb state, the atmospheric composition is altered to reflect the changes produced by the nuclear weapons tests. We have performed five separate experiments which will be briefly reviewed below.

The standard run, from which most of the illustrations are taken, is labeled the P experiment, where P stands for prognostic. In this run, the temperature and salinity fields in the interior of the model are entirely predicted by the model. Table 2 of part 1 shows global mean temperatures and salinities at the 12 model depth levels, both observed and predicted by the prognostic model. The A, B, and C experiments are semidiagnostic. Interior temperatures and salinities are restored toward observed values with a governing time constant of 1/50 $year^{-1}$.

Vertical mixing in the C experiment is parameterized by a uniform diffusion coefficient of 1.0 $cm^2\ s^{-1}$, while in the A, B, and P experiments the vertical mixing coefficient gradually increases from a value of 0.3 $cm^2\ s^{-1}$ in the upper kilometer to a value of 1.3 $cm^2\ s^{-1}$ in the lower kilometer. The A experiment uses a uniform gas exchange rate equivalent to 20 mol $m^{-2}\ yr^{-1}$ of CO_2, while the B, C, and P experiments use a wind speed dependent gas exchange rate which is mapped in Figure 3 of part 1. The wind-speed dependent gas exchange formulation assumes that the gas exchange rate in ice-covered areas is zero. Experiment P′ is identical to P except that the wind speed dependent gas exchange rates are increased by 20% over those used in P, B, and C. The different parameters of the five experiments are summarized in Table 4 of part 1.

Addition of Bomb ^{14}C to the Model

During the 1950s and early 1960s atmospheric tests of nuclear weapons produced enough new ^{14}C to nearly double the concentration of $^{14}CO_2$ in the atmosphere over natural, prebomb levels. Immediately after the bomb tests, the ocean began to absorb the bomb-produced ^{14}C. At present, atmospheric concentrations are only 15–20% above the prebomb background. The residence time for atmospheric CO_2 molecules with respect to exchange with CO_2 molecules in the upper ocean is fairly long, about 7–10 years [*Craig*, 1957]. The slow exchange rate allowed the $^{14}CO_2$ molecules produced by the bomb tests to become nearly homogenized within the atmosphere before significant exchange with the ocean occurred.

In part 1 the $^{14}C/^{12}C$ ratio of the atmosphere was held constant at pre-industrial and prebomb levels for the entire run. In part 2 the atmospheric $^{14}C/^{12}C$ ratio was varied as a function of time over the period 1950 through 1990 in accord with the observations. Figure 1 shows the model's atmospheric time history curve. During the years of active bomb ^{14}C production from 1954 to 1962 and for a few years afterward, atmospheric concentrations are divided among three broad latitude bands to include a small amount of atmospheric inhomogeneity. We have extrapolated the slowly declining part of the curve for the 1970s and early 1980s through 1990.

The gas exchange formulation in the model transfers ^{14}C to the ocean according to the local gas exchange rates and the difference between the specified atmospheric ^{14}C level and the predicted ^{14}C concentration in the surface layer. The governing equations for gas exchange are given as equations (10) and (11) in part 1.

Carbon 14 measurements are presented as a deviation (in parts per thousand, or per mil) from the $^{14}C/^{12}C$ ratio in the ^{14}C isotopic standard. For the purposes of this paper this is a convenient notation because the reference $^{14}C/^{12}C$ ratio (defined as 0‰) is approximately the $^{14}C/^{12}C$ ratio in the pre-industrial, prebomb atmosphere. An ocean value of −50 thus represents a 5% depletion in the $^{14}C/^{12}C$ ratio relative to the atmospheric levels of part 1. At the peak, bomb ^{14}C concentrations in the atmosphere reached 900‰, a 90% enrichment relative to pre-industrial time. We often refer to model ^{14}C output in the paper as "concentrations." Because there are no biological and chemical transformations of $^{12}CO_2$ or $^{14}CO_2$ in the model, model "concentrations" are equivalent to $^{14}C/^{12}C$ ratios.

Model Results at the Time of GEOSECS

North-South Sections

Figures 2, 3, and 4 show north-south sections of both observed and modeled ^{14}C concentrations along the western Pacific, western Atlantic, and eastern Indian GEOSECS tracks, respectively. The model results correspond in time to the years of the GEOSECS cruises. Values in excess of 0‰ are shown with dense stippling. The model results in Figures 2 and 3 can be laid over the prebomb results for the P model in Figures 10 and 11 of part 1 in order to assess the limits of bomb ^{14}C penetration. Prebomb values in the upper ocean are typically about −40‰, such that areas of the sections with ^{14}C contents much greater than −40‰ are heavily contaminated with bomb ^{14}C. Values in excess of −80‰ generally contain some bomb ^{14}C. In the Antarctic circumpolar region, bomb contamination extends to areas with values as low as −120‰.

Model results generally reproduce the depth of the 0‰ contour in the observations quite well. In each of the observed and modeled sections the ^{14}C contours trace out a deeper penetration of bomb ^{14}C in subtropical latitudes compared with tropical and polar latitudes. On closer inspection there are a number of deviations between the model and the GEOSECS data. The vertical penetration of the 0‰ contour north of 60° in the North Atlantic is much deeper in the model than in the observations, while in the subtropical North Atlantic the maximum penetration of the model's 0‰ contour is about 200 m shallower. This result is similar to the results of *Sarmiento* [1983], who found much the same

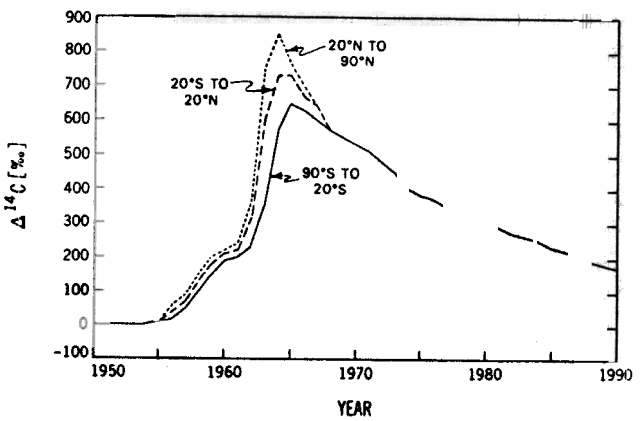

Fig. 1. Time history of atmospheric $\Delta^{14}C$ (per mil) between 1950 and 1990 used by the model (adapted from *Broecker et al.* [1980]).

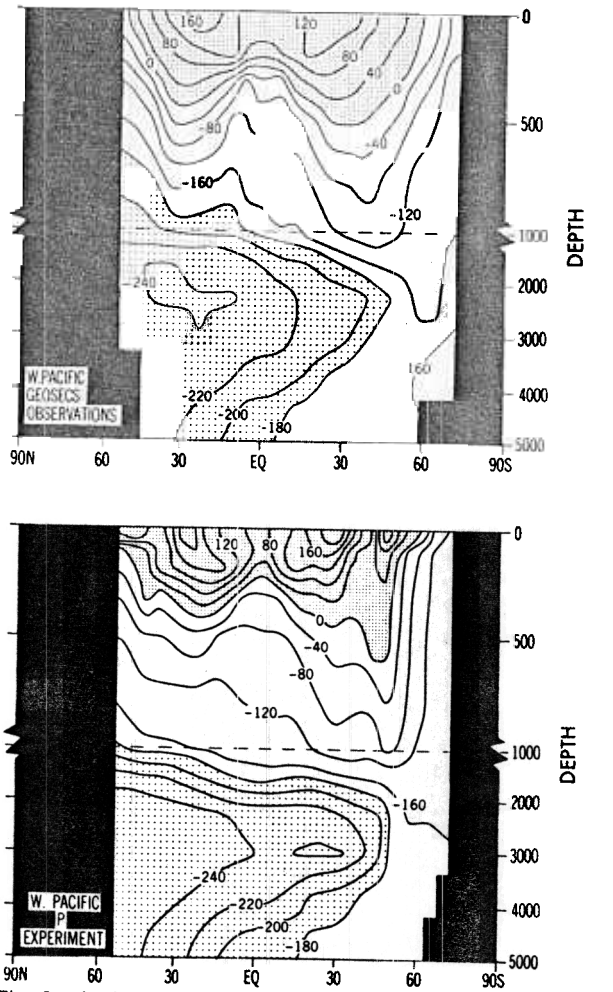

Fig. 2. Latitude versus depth sections of $\Delta^{14}C$ (per mil) along the western Pacific GEOSECS track: (top) GEOSECS observations and (bottom) P model prediction for 1974. The upper kilometer is shown with an expanded scale.

pattern in the penetration of tritium into the GFDL model. The Pacific sections show a lobe of bomb-contaminated water near 45°S in the model which is not found in the observations. The observed distribution of bomb ^{14}C in the Indian Ocean shows a striking contrast between deep penetration in the subtropical latitudes south of the equator and relatively shallow penetration near the equator itself. Although the maximum penetration of bomb ^{14}C near 40°S is deeper in the model than in the GEOSECS section, the steep north-south gradient in bomb ^{14}C near 15°S is captured very well by the model.

While the two-dimensional comparisons of model results along the GEOSECS tracks with the observations represent a very straightforward form of model validation, they are not very helpful in illustrating how the distributions arise. Mechanisms are much better highlighted when results are presented in map form. Most of the results to follow will be presented this way, even though the maps of observations are constructed from data which are quite sparse.

Surface Water

Figure 5 shows a comparison of bomb ^{14}C surface concentrations between the GEOSECS observations and the P model. The top panel, reproduced from BPOS, maps the

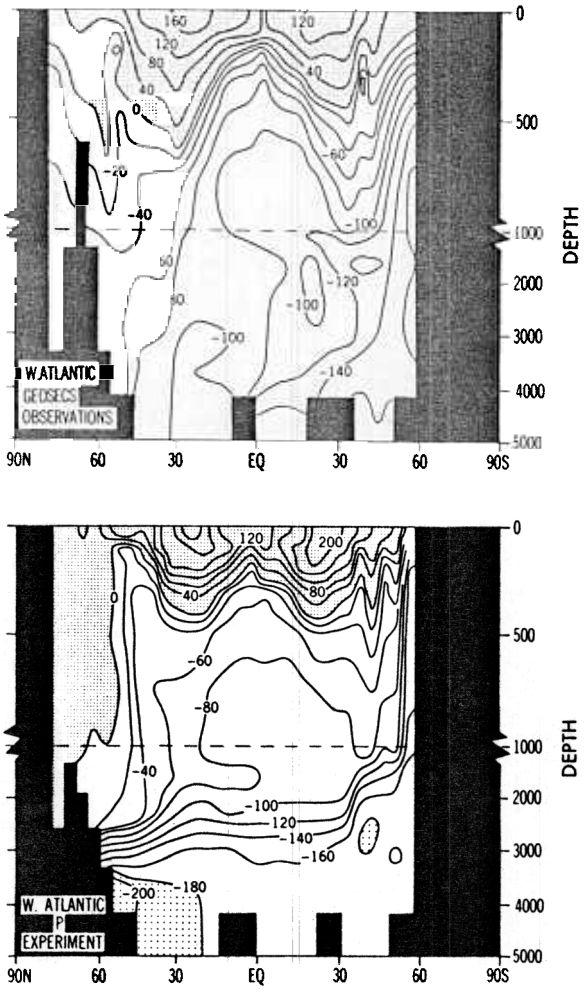

Fig. 3. Latitude versus depth sections of $\Delta^{14}C$ (per mil) along the western Atlantic GEOSECS track: (top) GEOSECS observations and (bottom) P model prediction for 1972.

difference between the measured GEOSECS surface ^{14}C and the estimated prebomb surface values. The BPOS analysis shows that surface ^{14}C values in the equatorial belts of all three ocean basins are distinctly lower than surface values in the adjacent subtropical belts. BPOS attribute the lower equatorial values to the upwelling of water at the equator which had not been contaminated with bomb ^{14}C at the time of GEOSECS. The highest observed bomb ^{14}C concentrations at the time of GEOSECS (>200‰) are found in subtropical latitudes of both hemispheres of the eastern Pacific, and in the central North Atlantic.

The observed mean concentration of bomb ^{14}C in surface water is 160‰ [*Broecker et al.*, 1980]. The P model predicts a mean concentration of 159. The model appears to locate the surface maxima and minima in the right places. Predicted values of the maxima, however, appear to be much too high, and the minimum values in the equatorial Pacific and Indian oceans are too low. The model predicts very high values between South America and 120°W in the South Pacific, an area for which there are no GEOSECS points for comparison. The model predicts high surface values in the eastern South Atlantic in an area where there are no measurements as well. One of the worst deficiencies in the model occurs in the far North Pacific, where model ^{14}C concentrations are 50–60‰ higher than observed.

Bomb ^{14}C surface concentrations highlight the most rapidly responding parts of the system. The high surface values near the eastern boundaries of the Pacific are tracking surface water masses which were drifting eastward under the westerly winds during the time of high atmospheric ^{14}C concentrations. These surface flows turn equatorward near North and South America. The denser water masses from the north become subducted into the upper thermocline as they move south. In the North Pacific, the subducted water masses have temperatures between 10° and 20°C [*Reid*, 1973]. These water masses carry a well-defined maximum of ^{14}C and tritium into the thermocline. This maximum is evident south of Hawaii in both the observations (GEOSECS 235) and in the model ^{14}C simulations.

The model predicts surface water bomb ^{14}C concentrations in the Pacific off North America in excess of 320‰ during 1974, whereas the GEOSECS data in this area record maximal values of 260‰. It is worth pointing out that the highest bomb ^{14}C concentration ever recorded (315‰) came from a subsurface (75 m) sample collected in this area (at the location of GEOSECS 347) during 1969 [*Ostlund and Niskin*, 1970; *Broecker and Peng*, 1980].

Figure 6 shows a comparison between predicted surface

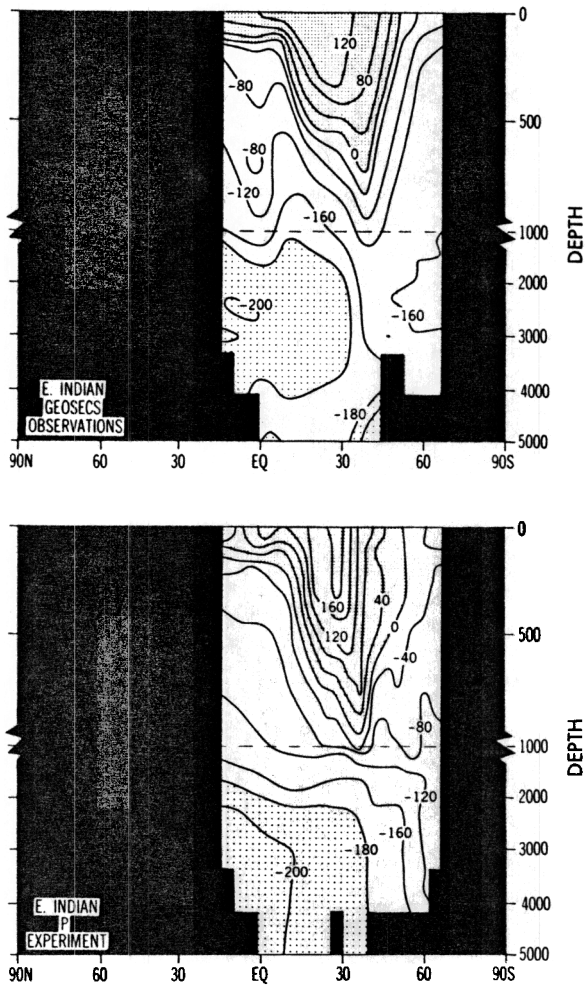

Fig. 4. Latitude versus depth sections of $\Delta^{14}C$ (per mil) along the eastern Indian GEOSECS track: (top) GEOSECS observations and (bottom) P model prediction for 1978.

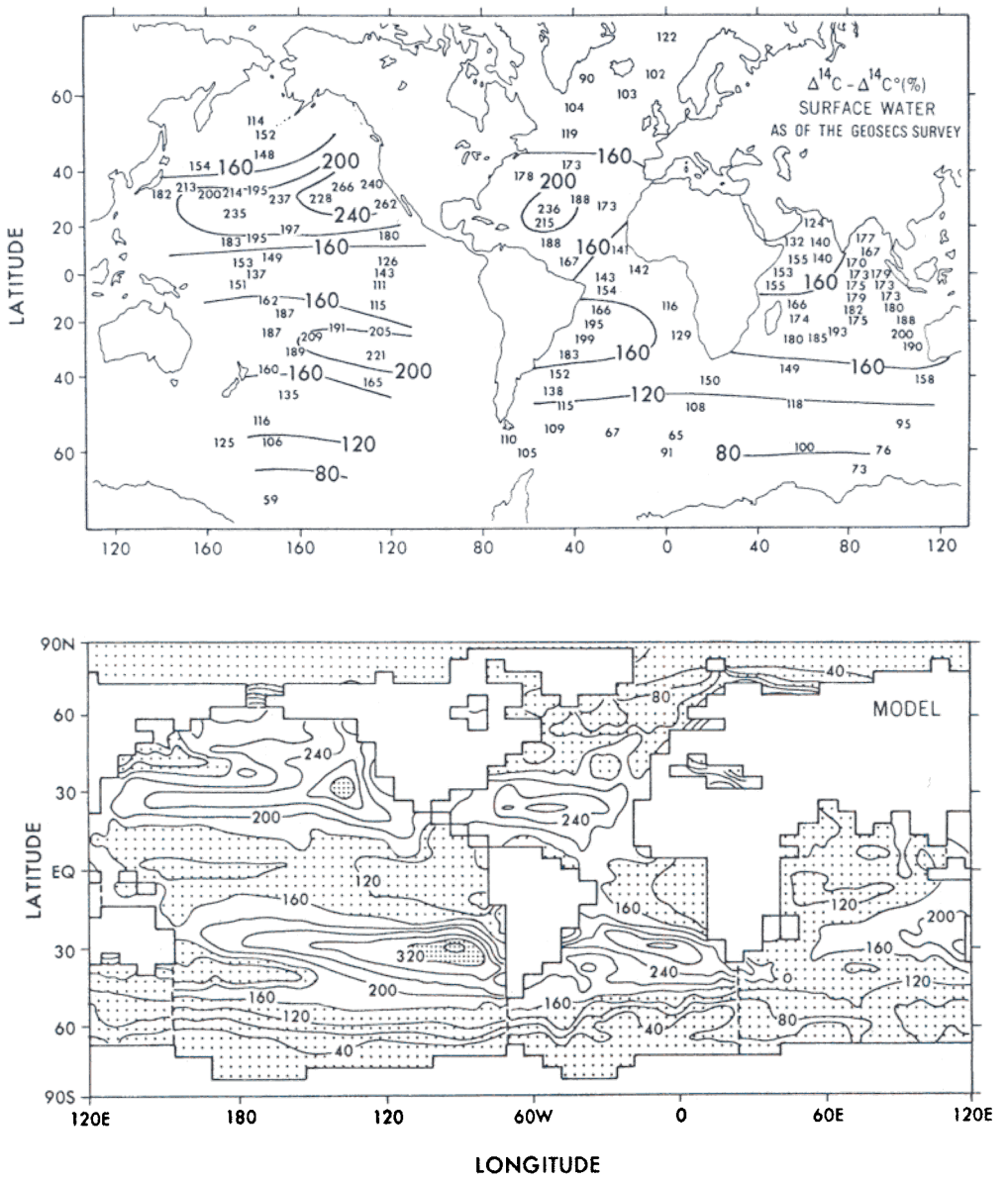

Fig. 5. Bomb ^{14}C content of surface water (per mil) at the time of the GEOSECS surveys. The bomb ^{14}C content is defined as the difference between the $\Delta^{14}C$ at the time of GEOSECS and the prebomb $\Delta^{14}C$. The top panel shows the GEOSECS observations as compiled by *Broecker et al.* [1985]. The bottom panel shows the output of the P model for the years 1972 (Atlantic), 1974 (Pacific), and 1978 (Indian). Contours have been added to Broecker et al.'s original map to help highlight comparisons with the model results.

water ^{14}C concentrations from the B and C experiments which illustrates the effect of vertical mixing on surface bomb ^{14}C concentrations. Results from *Broecker and Peng* [1982] summarize the observations. The B and C models are identical in all respects except for their vertical mixing parameterizations. The B model, like the P model, uses a mixing coefficient of 0.3 $cm^2\ s^{-1}$ in the upper kilometer, while the C experiment uses a coefficient of 1.0 $cm^2\ s^{-1}$.

While the B model's surface concentrations in Figure 6 are much too high in the subtropics, the predictions for the equatorial regions are in good agreement with the observations. On the other hand, the C model predicts subtropical surface concentrations which are about right, but it grossly underpredicts the observed concentrations in the equatorial regions. These results suggest that the mixing coefficient used in the B (and P) experiment is much too small to simulate the effects of wind stirring and seasonal convection beneath the mixed layer in subtropical latitudes. A generally larger mixing coefficient, however, is no solution because it would overestimate the extent of mixing in the more strongly stratified tropical oceans. These results suggest that a more complex parameterization of vertical mixing in the upper ocean may be necessary.

Bomb ^{14}C Inventories

The inventory of bomb ^{14}C at a given location is defined as the amount of ^{14}C present in excess of the prebomb concentrations. It is determined by integrating the difference between prebomb and postbomb vertical profiles. Differences in ^{14}C between the postbomb and prebomb simulations of the P model are used to produce a map showing the distribution of bomb ^{14}C inventories at the time of GEO-

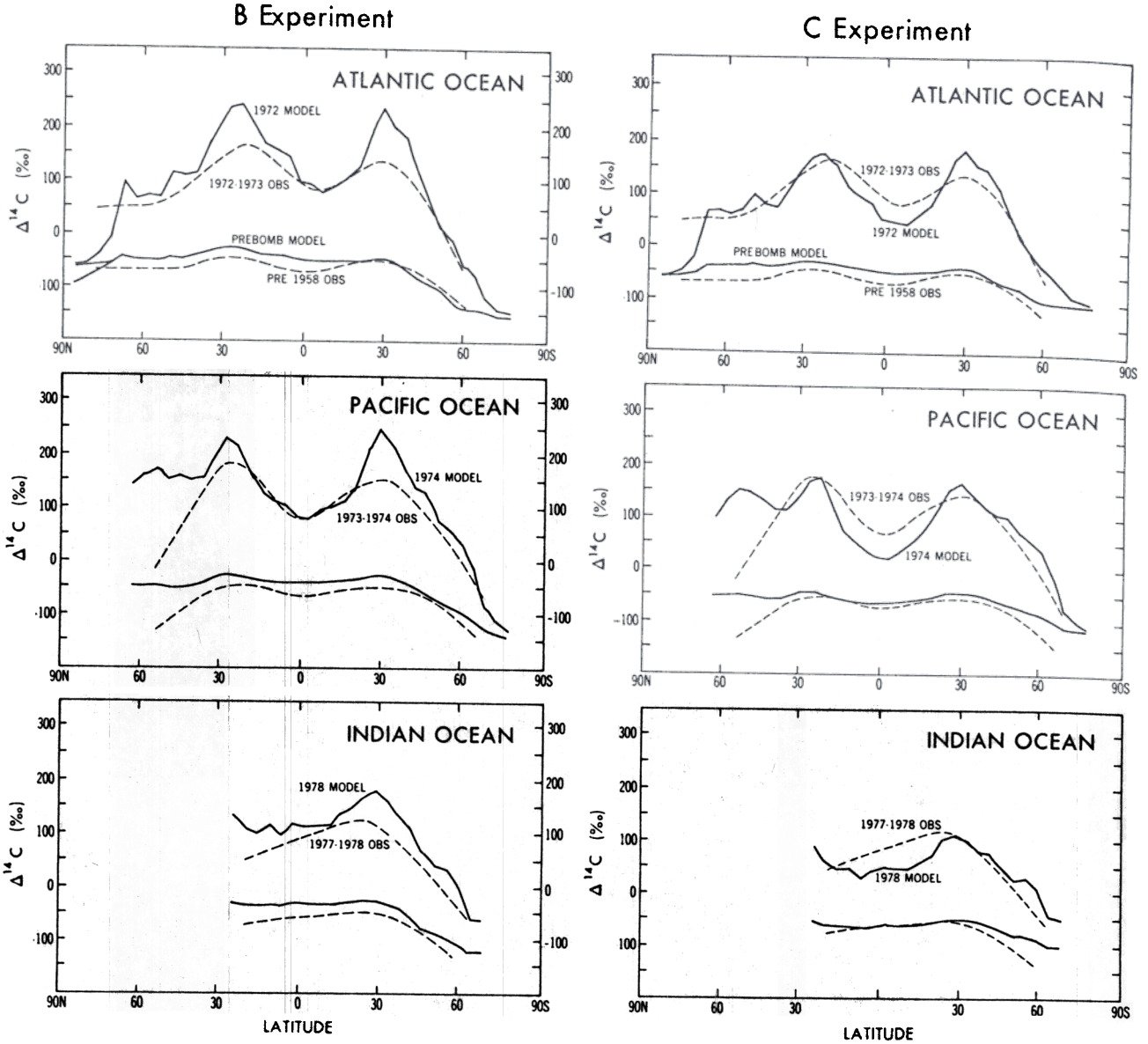

Fig. 6. Comparison between the predicted zonally averaged surface values of $\Delta^{14}C$ in the B and C models (solid lines) and the GEOSECS observations (dashed lines) for the Atlantic, Pacific, and Indian Oceans. Zonal mean observations have been redrawn from *Broecker and Peng* [1982].

SECS. Figure 7 shows a comparison between the BPOS analysis of the GEOSECS data and the model's prediction. An average CO_2 concentration of 2.15 mol m^{-3} was used to convert model ^{14}C units into ^{14}C inventories. Use of this average CO_2 concentration overestimates inventories in warm water and underestimates inventories in cold water by a few percent.

The BPOS analysis shows that bomb ^{14}C inventories between 15° and 45° latitude in both hemispheres are 2 to 5 times higher than inventories in the adjacent equatorial and subpolar regions. BPOS argue that to a first approximation, the number of atoms of bomb ^{14}C entering the ocean through each unit of the ocean's surface up to the time of GEOSECS is fairly uniform. The spatial structure in the bomb ^{14}C inventory maps thus reflects a large-scale redistribution of bomb ^{14}C after it has come into the ocean. As with surface concentrations, there is a noticeable symmetry in the inventory distributions about the equator, particularly in the Pacific. In contrast to the surface concentrations, the largest bomb ^{14}C inventories are generally found near the western margins of the major ocean basins. These areas coincide with the areas of intense recirculation in the subtropical gyres where the thermocline is most strongly depressed.

The model has little difficulty reproducing the gross displacement of bomb ^{14}C inventories from the equatorial and high-latitude regions into the subtropics. On a finer scale, however, there are significant differences between the model results and observations. The largest model inventories tend to coincide with the areas of high surface concentration near the eastern margins. This occurs for two reasons. As noted above, the maximum model surface concentrations tended to be too high, skewing inventory maxima toward areas of high concentrations. Also, the depths to which bomb ^{14}C penetrates in the recirculation regions of the subtropical gyres are too shallow, as was noted by *Sarmiento* [1983] with respect to the tritium penetration in the North Atlantic.

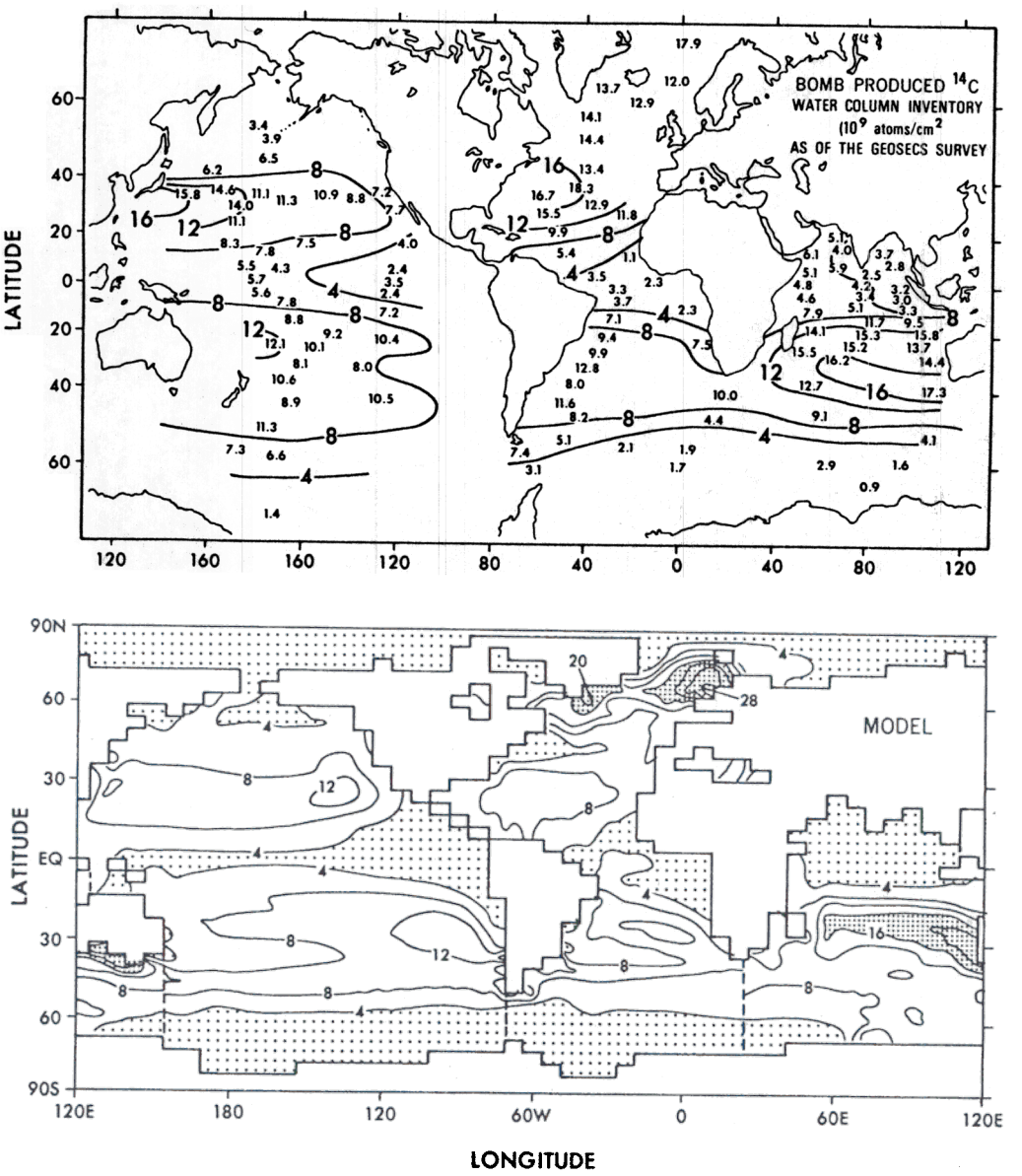

Fig. 7. Vertically integrated inventories of bomb ^{14}C (10^9 atoms ^{14}C cm^{-2}) at the time of GEOSECS. The top panel shows the GEOSECS observations as compiled by *Broecker et al.* [1985]. The bottom panel shows the output of the P model for the years 1972 (Atlantic), 1974 (Pacific), and 1978 (Indian). Contours have been added to the Broecker et al. map to facilitate a comparison with model results.

Model inventories in the Norwegian Sea are much higher than observed inventories. Recall from Figure 3 that the model produced a very strong bomb ^{14}C penetration to the bottom in this area, while the observations show a much lower level of penetration in deeper levels. The model convects to the bottom in the eastern part of the Norwegian Sea, accounting for the large inventory buildup in Figure 7. A recent paper by *Swift and Koltermann* [1988] shows that the deep water of the Norwegian Sea does not form from local convection. It forms instead from an inflow of deep water from the Greenland Sea and Arctic Ocean, such that the buildup of bomb ^{14}C concentrations in the deep Norwegian Sea is not very fast.

One of the model's most serious deficiencies shows up clearly in the tongue of low-inventory water extending eastward from North America in the North Atlantic. From an analysis of a numerical circulation model run by *Holland* [1971], *Veronis* [1975] pointed out that models with lateral mixing oriented strictly along horizontal surfaces tend to produce an artificial upwelling of deep water on the landward side of strong western boundary currents. In the present model the upwelled water spreads to the east, displacing a great deal of bomb ^{14}C inventory to the north. Although not as obvious, tongues of low inventory also extend eastward from Australia and Asia in the Pacific and from South America in the South Atlantic.

The Indian Ocean proves an exception to the pattern of the other oceans. The observations show a tongue of high inventory extending westward from the coast of Australia. This tongue is reproduced by the model but at a slightly more tropical latitude. Much of the bomb ^{14}C inventory in this tongue is well below the surface, in contrast to other areas of high inventory. This process appears to be most vigorous in the Indian Ocean, although the later date (1978 versus 1972

TABLE 1. Summary of Bomb ^{14}C Inventories by Region

Region	10^9 atoms cm^{-2}						Fractional Area
		Model					
	Observed*	P	B	C	P′	A	
Atlantic (1972)							
Subarctic (45°–75°N)	13.8	11.0	8.6	9.9	12.7	8.7	0.032
North temperate (15°–45°N)	13.2	7.1	7.7	7.7	8.2	8.9	0.068
Equatorial (15°S to 15°N)	3.5	3.8	4.0	3.9	4.4	5.0	0.048
South temperate (15°–45°S)	9.5	8.4	8.1	8.7	9.6	8.0	0.062
Antarctic (>45°N)	2.1	4.0	3.7	4.7	4.6	4.7	0.047
Pacific (1974)							
Subarctic (45°–65°N)	5.9	4.6	4.0	6.8	5.3	4.2	0.028
North temperate (15°–45°N)	9.3	8.5	8.5	8.9	9.7	9.6	0.121
Equatorial (15°S to 15°N	5.7	4.4	4.5	4.4	5.0	5.8	0.149
South temperate (15°–45°S)	11.0	8.6	8.5	8.7	9.7	9.3	0.129
Antarctic (>45°N)	5.9	5.0	6.1	7.0	5.8	5.9	0.071
Indian (1978)	8.5	8.6	8.1	8.7	9.9	9.1	0.220
Arctic (1972)	4	1.4	1.5	1.4	1.6	7.1	0.026
Averages†	8.2	6.9	6.8	7.3	7.9	7.8	

*Compiled by *Broecker et al.* [1985]
†Averages are area weighted.

and 1974) and better three-dimensional coverage of the Indian Ocean GEOSECS survey may also help make it more noticeable.

Table 1 summarizes bomb ^{14}C inventories produced by all five model experiments by region and compares these results with the GEOSECS inventories compiled by BPOS. BPOS concluded that the ocean contained about 2.9×10^{28} atoms of bomb ^{14}C at the time of GEOSECS, which if divided by the ocean's area yields an average bomb ^{14}C inventory of 8.2×10^9 atoms cm^{-2}. The P model's average inventory is 6.9×10^9 atoms cm^{-2}, about 16% less. The C model with more vertical mixing takes up slightly more, 7.3×10^9 atoms cm^{-2}.

The model's low bomb ^{14}C inventories could be explained by one of two factors. Either the input of bomb ^{14}C by gas exchange is too weak, or the processes which give rise to the vertical penetration of bomb ^{14}C are not vigorous enough. *Broecker et al.* [1980] point out that higher rates of gas exchange or more vigorous vertical mixing will increase bomb ^{14}C inventories but will have opposite effects on surface ^{14}C concentrations. More vigorous vertical mixing acts to increase the model's bomb ^{14}C inventories by removing bomb ^{14}C from the surface layer, thereby lowering surface concentrations and increasing the ocean-atmosphere ^{14}C gradient. Higher rates of gas exchange will allow more ^{14}C to enter the ocean, but will raise surface ^{14}C concentrations. As pointed out earlier, the model's global average surface concentration at the time of GEOSECS is very close to the observed average. We have concluded that the P model's relatively low inventories can best be explained by low gas exchange rates. However, if real gas exchange rates are indeed higher than the values used by the P model, more mixing in the upper ocean is needed to satisfy both constraints.

The gas exchange rates used in the model were computed from a correlation between local wind speed and CO_2 invasion rate published by BPOS, combined with estimates of annual mean wind speeds over the ocean compiled by *Esbensen and Kushnir* [1981]. The global mean gas exchange rate computed this way is 16.6 mol CO_2 m^{-2} yr^{-1}. One-dimensional model calculations [*Oeschger et al.*, 1975; *Broecker et al.*, 1980] require gas exchange rates of about 20–21 mol CO_2 m^{-2} yr^{-1} to fit the globally averaged vertical profiles of ^{14}C in the ocean. For our P′ experiment we increased the local gas exchange rates used by the P experiment by 20% and found that this model produced a global inventory of 7.9×10^9 atoms cm^{-2}, in much better agreement with BPOS. However, the P′ experiment's average surface concentration at the time of GEOSECS is 180‰, 20‰ higher than observed.

Given the effects of vertical mixing on surface concentrations illustrated in Figure 6, we argued that a mixing coefficient of 0.3 cm^2 s^{-1} is simply too small to represent the effects of wind stirring and seasonal convection in the subtropics. The best possible simulation with an annual mean model of this type requires the higher gas exchange rates used by the P′ model to get more bomb ^{14}C into the ocean and more vigorous vertical mixing in the upper few hundred meters of the subtropics to hold surface ^{14}C concentrations down.

POST-GEOSECS MODEL PREDICTIONS

Figure 8 displays a series of maps which illustrate how bomb ^{14}C inventories change over time in the P model. The maps in Figure 8 correspond to the model's predictions of what would have been observed from repeated global surveys at 9-year intervals. The top map shows bomb ^{14}C inventories in 1972. As such, the top panel is similar to the model output in Figure 7 except that all results are for 1972 instead of the individual GEOSECS years.

Between 1972 and 1981 the symmetrical pattern of inventory accumulation between the northern and southern hemispheres, which was noted in the observations by BPOS, is no longer evident in the model. The parts of the North Pacific which accumulated the largest inventories prior to 1972 begin to lose bomb ^{14}C. Relatively large increases in inventory occur between 40° and 65° in the North Atlantic and in the middle latitudes of each of the southern hemisphere ocean basins. Large inventory increases continue in

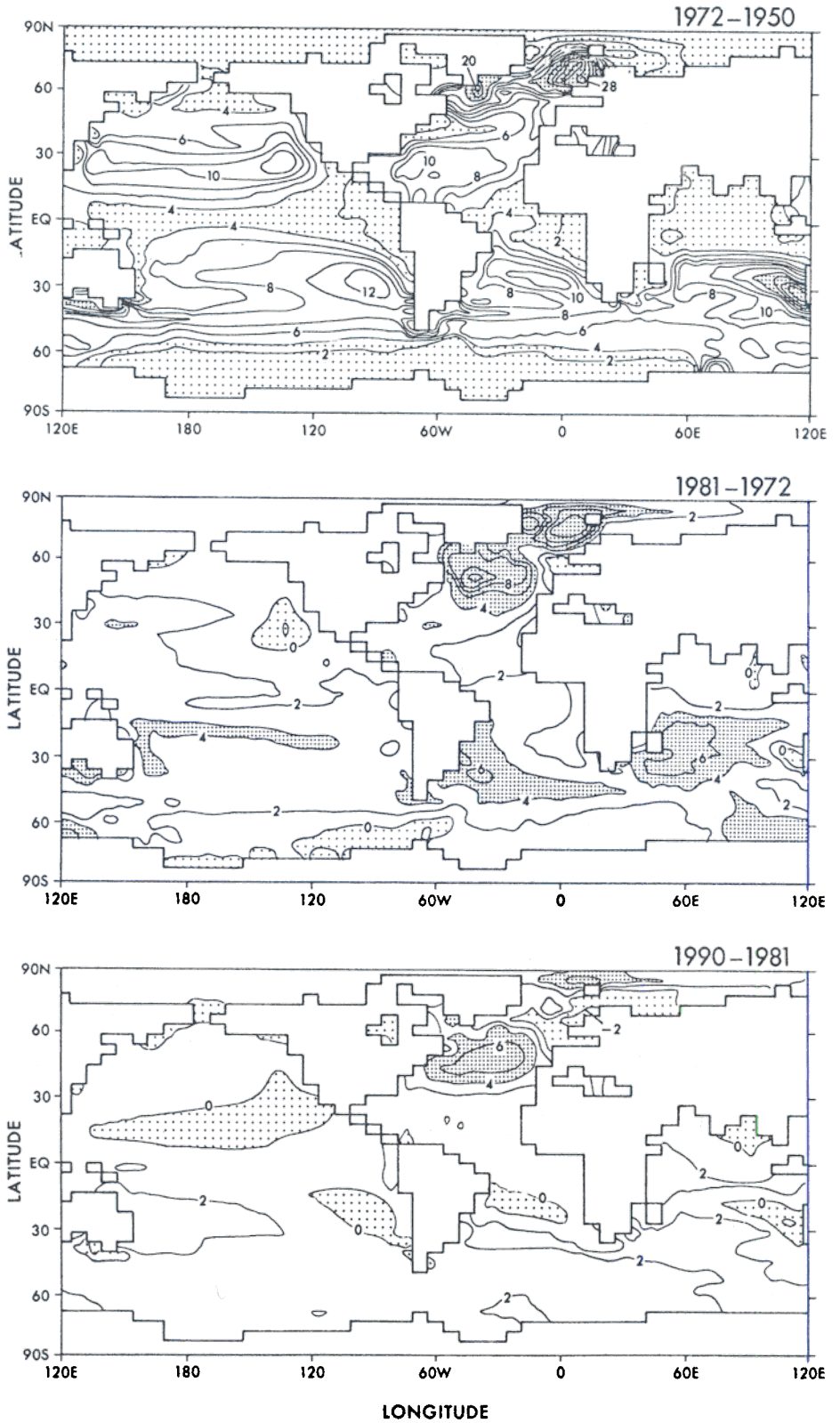

Fig. 8. Predicted changes in bomb ^{14}C inventories (10^9 ^{14}C atoms cm^{-2}) for the P model between 1972 and 1990. The top panel shows the difference between ^{14}C concentrations in 1972 and the prebomb equilibrium. The middle and bottom panels show the differences between ^{14}C concentrations in 1981 and 1972 and between those in 1990 and 1981, respectively. Please note that although the contour intervals are the same in all three time periods (2×10^9 atoms cm^{-2}), the stippling convention in the top panel is different from the convention in the bottom two panels.

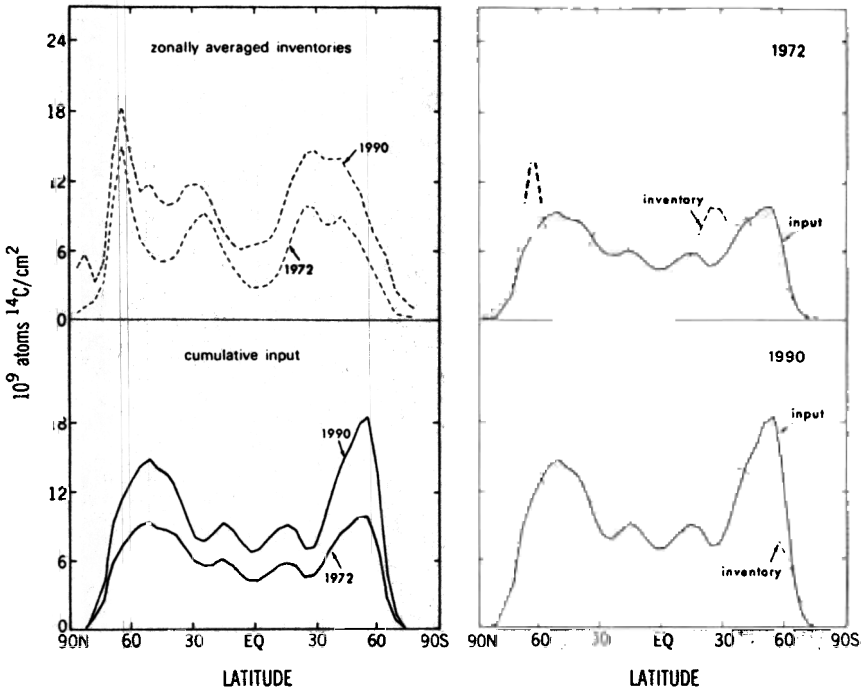

Fig. 9. Comparison of cumulative bomb ^{14}C inputs through each model grid box with bomb ^{14}C inventories residing in the local water column, plotted as zonal averages (units are 10^9 ^{14}C atoms cm^{-2}). Left-hand panels show (top) inventories in 1990 and 1972 and (bottom) cumulative inputs up through 1972 and 1990 for the P model. Right-hand panels replot the same results so as to compare inventory and cumulative inputs for same time periods, (top) 1972 and (bottom) 1990.

the Norwegian Sea. The equatorial regions are not nearly as conspicuous for their lack of inventory accumulation. Between 1981 and 1990, large areas of the North Pacific lose inventory. Virtually all the areas of high inventory in 1972, including the Norwegian Sea, lose inventory. The North Atlantic between 35° and 60°N and part of the Arctic Ocean gain inventory at the greatest rate. Broad areas of the South Pacific and southern Indian Ocean accumulate more than 2 $\times$ 10^9 atoms cm^{-2} of bomb ^{14}C.

Between 1972 and 1981 the atmosphere–ocean surface contrast in ^{14}C content is less than half what it was during the previous decade. Thus the overall uptake of bomb ^{14}C by the ocean is much reduced during this time interval. By 1990, model surface waters in small areas of the mid-latitude gyres have surface ^{14}C contents which actually exceed the atmosphere's ^{14}C content, which we have estimated to be about 170‰. As atmosphere-ocean differences in bomb ^{14}C concentration decline over time, the ocean uptake dominated by huge and fairly uniform inputs prior to GEOSECS shifts to emphasize uptake in areas where surface ^{14}C concentrations remain low. Figure 9 summarizes the contrast between where bomb ^{14}C enters the ocean and where it resides. During the bomb ^{14}C integration the model keeps track of the input of bomb ^{14}C from the atmosphere in each surface grid box. In Figure 9 we have zonally integrated the cumulative inputs up to 1972 and up to 1990 and plotted these results along with zonal integrals of the bomb ^{14}C inventories shown in Figure 8.

Prior to 1972, the input of bomb ^{14}C is relatively constant with latitude, except in the areas where sea ice cuts off gas exchange. Between 1972 and 1990 the input of new ^{14}C from the atmosphere is concentrated in higher latitudes, particularly in the circumpolar belt between 40°S and 60°S. A map of the ocean-atmosphere ^{14}C gradient for 1990 (not shown) shows that in addition to the circumpolar region and North Atlantic, the eastern equatorial Pacific and equatorial Indian continue to have significant inputs of bomb ^{14}C 30 years after the bomb tests.

The largest increases in inventory between 1972 and 1990 occur between 30°N and 55°N and between 20°S and 50°S. The equatorial regions, particularly south of the equator, accumulate a significant amount of new inventory as well. Virtually all of the inventory increase in the northern hemisphere between 1972 and 1990 takes place between 30° and 60°N in the North Atlantic, as can be seen in Figure 8. Much of the largest inventory increase occurs in a latitude belt which had a minimum of inventory in 1972. The post-1972 buildup of inventory in this area represents, in part, a filling in of the deep source waters for the model's spurious western boundary upwelling.

In the southern hemisphere there is a distinct northward shift of bomb ^{14}C. Bomb ^{14}C which entered the ocean in the circumpolar belt has moved to lower latitudes. The shift is evident by 1972 but is especially significant by 1990. BPOS describe the buildup of inventory in the temperate latitudes of the southern hemisphere as a consequence of a generalized downwelling of surface waters which had been transported laterally into the zone of mid-latitude convergence. In the GFDL model this transfer occurs by deep convection along the northern edge of the circumpolar current followed by northward spreading into the southern hemisphere thermocline. This process is examined in more detail in the next section.

In 1972, bomb ^{14}C inventories in the equatorial belt are distinctly lower than the cumulative inputs, as pointed out by BPOS. By 1990, equatorial inventories have almost

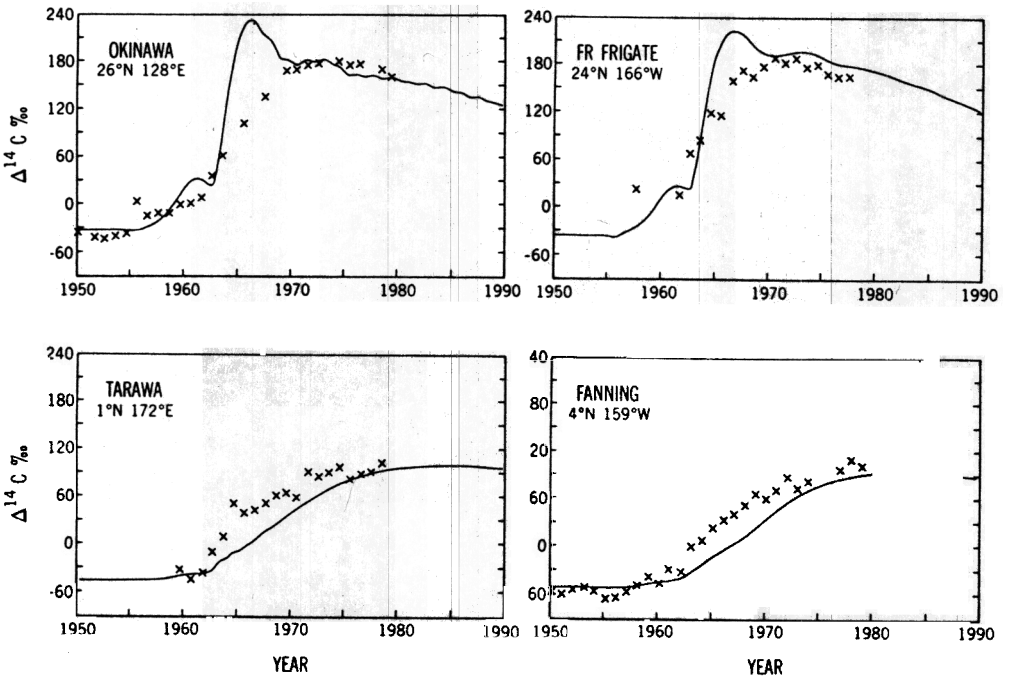

Fig. 10. Comparison of observed and modeled bomb ^{14}C time histories in surface waters of the North Pacific. Data and model results from Okinawa and French Frigate Shoals, in the subtropical North Pacific, and from Tarawa and Fanning Islands, in the equatorial North Pacific, are shown. Okinawa data are taken from *Konishi et al.* [1982]. French Frigate Shoals and Fanning Island data are taken from *Druffel* [1987]. Tarawa data are taken from *Toggweiler* [1983]. Model curves are from the P model.

caught up with the cumulative input. This is explained in the context of the overturning diagram in Figure 4 of part 1. In the early years after the bomb tests, the water upwelling in the equatorial regions was largely devoid of bomb ^{14}C. However, the water feeding the equatorial upwelling systems comes from quite shallow depths [*Fine et al.*, 1981; *Quay et al.*, 1983], such that by the second postbomb decade, the upwelling water has been largely saturated with bomb ^{14}C input. The cycling of water through the equatorial regions thus brings in as much ^{14}C as is taken out, and the large-scale displacement of bomb ^{14}C identified by BPOS ceases.

Figure 10 shows a comparison between time series measurements of surface water ^{14}C as recorded by banded corals and model predicted time series at four locations, two near the equator in the central Pacific (Fanning and Tarawa), and two in the subtropics of the North Pacific (Okinawa and French Frigate Shoals). These comparisons show that the buildup of bomb ^{14}C in subtropical surface water during the mid-1960s is much faster in the model than in observations. At the same time, the buildup of bomb ^{14}C in the model tropics lags behind the observed buildup. By the late 1970s, model surface levels are in good agreement with observed ^{14}C levels. This comparison shows that the time required for the model to cycle water from the subtropics through the equatorial upwelling system is too long. *Quay et al.* [1983] have estimated that only 4–6 years are required to flush subtropical water less than 300 m deep ($\sigma_\theta < 26.5‰$) through the equatorial upwelling system. The parameterized eddy mixing or eddy viscosity needed to maintain numerical stability in the model appears to retard the cycling of water between the tropics and subtropics by a few years.

Penetration of Bomb ^{14}C Into the Southern Hemisphere Thermocline

Figure 11 shows a series of snapshots of model ^{14}C concentrations at level 6 (755 m) for the southern hemisphere at 1972, 1981, and 1990. This series of maps graphically illustrates how the model's lower thermocline is ventilated in the southern hemisphere. In 1972 the presence of bomb ^{14}C is evident to the west of Australia in the Indian Ocean and to the south and east of Australia in the Pacific. By 1981 the Indian Ocean tongue is greatly expanded, and new tongues have appeared to the east and west of South America. By 1990, traces, at least, of bomb ^{14}C have filled in most of the area between 20°S and 60°S.

Bomb ^{14}C reaches level 6 initially in two zones of intense convection adjacent to Australia. Convection in these areas can be explained in terms of the surface forcing. The axis of the westerlies in the Indian Ocean sector of the circumpolar region lies between 42°S and 45°S [*Hellerman and Rosenstein*, 1983]. As wind velocities taper off north of this region, the shear in the wind produces convergent flow in the surface water over an immense area. The convergence pushes the surface water down and creates an upper layer with relatively low stability. Convection occurs along this belt in areas with slightly more dense surface water.

In the real ocean this latitude belt is a source of Subantarctic Mode Water [*McCartney*, 1977]. McCartney has documented the existence of very deep winter mixed layers (as deep as 600 m) within this region. *McCartney* [1982] showed that the water masses formed from these deep winter mixed layers (identified as minima in the local stratification) spread northward into the southern Indian and Pacific oceans. The

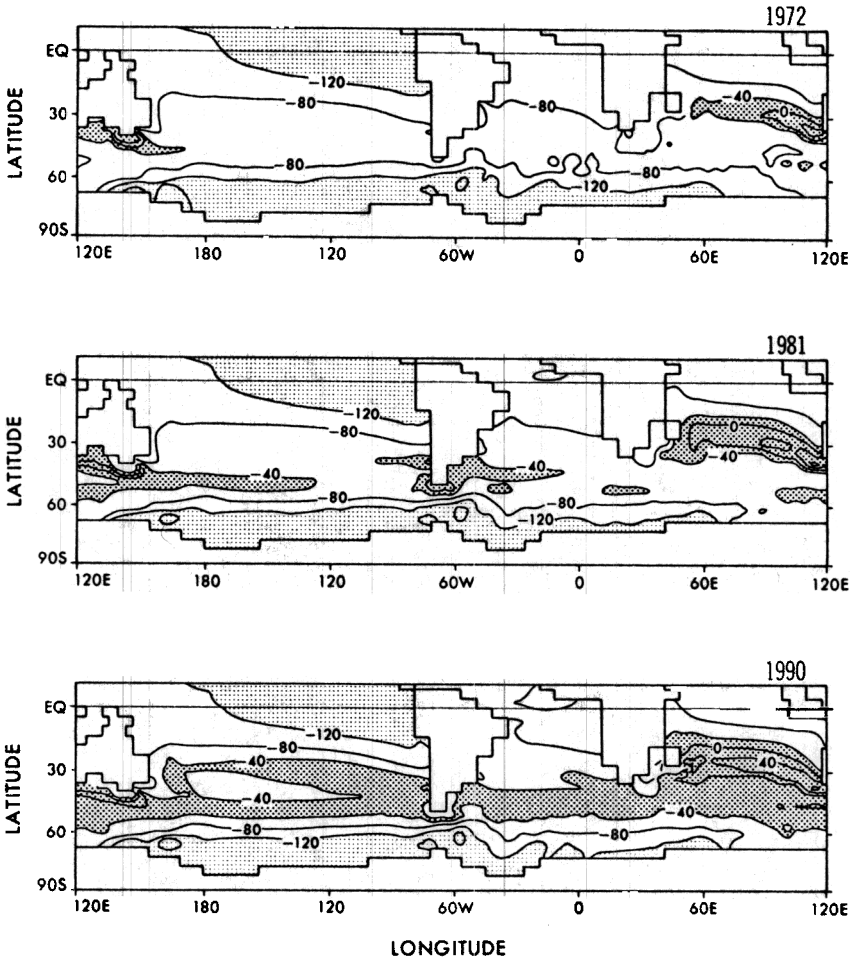

Fig. 11. Maps of predicted $\Delta^{14}C$ at level 6 (755 m) during (top) 1972, (middle) 1981, and (bottom) 1990 in the southern hemisphere of the P model. Carbon 14 values in excess of −40‰ are shaded with heavy stippling, indicating the presence of bomb ^{14}C.

model does not have any seasonal forcing, but it does produce convection in areas of low vertical stability. In the Indian Ocean the model forms a weakly stratified water mass which spreads to the north much like McCartney's Subantarctic Mode Water.

The French INDIGO expeditions in the Indian Ocean during 1985–1987 have reoccupied several GEOSECS stations (see Figure 12 for locations) and collected ^{14}C samples. Figure 13 shows model profiles and observed profiles at the location of GEOSECS 420, on the equator in the western

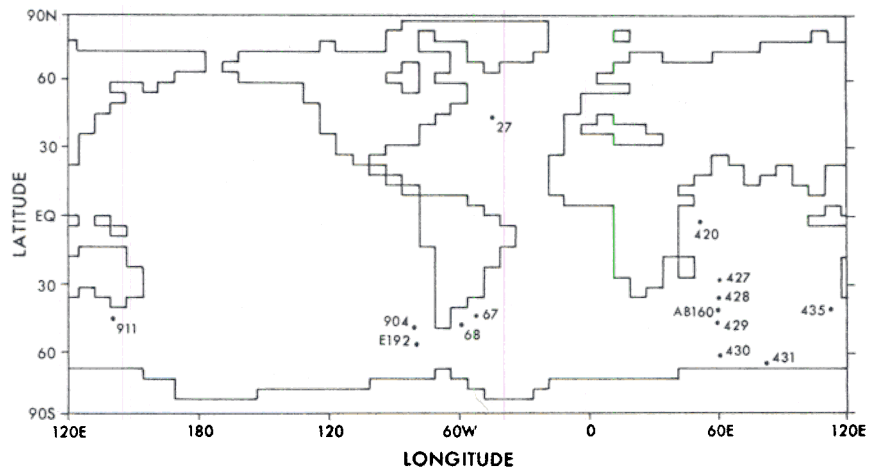

Fig. 12. Locations for vertical profiles and sections illustrated in the paper. Most of the locations in Figure 12 correspond to the locations of GEOSECS stations and are named accordingly. Two locations, 904 and 911, have been selected on the basis of important model features and have been given the names used in our analysis. AB160 and E192 represent stations from which *McCartney* [1977] documented deep winter mixed layers along the northern edge of the circumpolar current; these are *Anton Brunn* station 160 and *Eltanin* station 192, respectively.

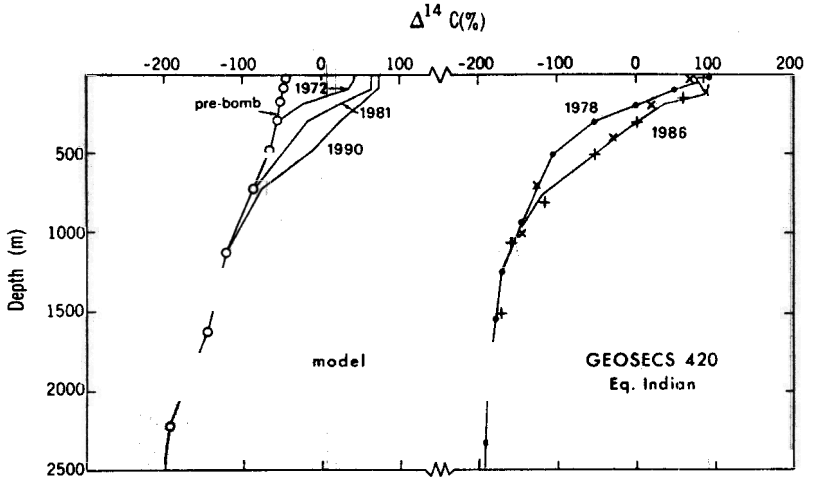

Fig. 13. Comparison between model predictions and observations of vertical profiles of bomb ^{14}C at the location of Indian Ocean GEOSECS station 420. (Left) Results for the P model are given for the pre-bomb equilibrium, 1972, 1981, and 1990. (Right) Data are shown for 1978 (GEOSECS 420; solid circles) and 1986 (INDIGO station 45; crosses [*Ostlund and Grall*, 1988] and pluses [*Bard et al.*, 1988]).

Indian Ocean. Model profiles are sampled from the prebomb equilibrium, and in 1972, 1981, and 1990. The water column at GEOSECS 420 was sampled in 1978 and again in 1986 as INDIGO 45 [*Bard et al.*, 1988; *Ostlund and Grall*, 1988]. The model predicts significant subsurface increases in bomb ^{14}C between 1972 and 1981 and between 200 and 1000 m after 1981. The observed increases between 1978 and 1986 are consistent with the model's prediction.

Bard et al. [1988] argue that the observed inventory build up between 1978 and 1986 can be attributed to bomb ^{14}C in Pacific water flowing through passages in the Indonesian archipelago. However, the water mass in which the greatest observed inventory increase occurs (300–500 m) coincides closely in density with Subantarctic Mode Water of circumpolar origin (σ_θ = 26.7–27.0 [*McCartney*, 1982]). *Bard et al.* [1989], using output from this model, show that both sources in the model contribute bomb ^{14}C to the equatorial Indian Ocean. The Pacific source is especially important in the upper 300 m where model densities are less than 26.0, while the circumpolar source dominates below 400 m where model densities are between 26.0 and 27.0.

The model produces a variation on the mode water concept in the South Pacific. The tongue of bomb ^{14}C extending westward from South America into the South Pacific in the 1981 snapshot of Figure 11 actually originates in the convection zone south of Australia. It travels eastward across the Pacific mainly above level 6 and is pushed down to level 6 by downwelling off South America (see Figure 14 in part 1). The model thus generates a weakly stratified water mass which spreads into the South Pacific, but it does not generate this water mass in the right place or with the right temperature-salinity (*T-S*) properties. A second convection center in the South Pacific near the date line penetrates to level 5 and contributes bomb ^{14}C to the downwelling off South America. The strong downward penetration of bomb ^{14}C near Australia and subsequent eastward transport account for the spurious lobe of bomb ^{14}C at 45°S in Figure 2.

The bomb ^{14}C seen spreading from the other side of South America into the Atlantic in the 1981 snapshot does not reach level 6 locally either. The bomb ^{14}C in this tongue comes through the Drake Passage at shallower levels and is pushed downward by downwelling on the Atlantic side.

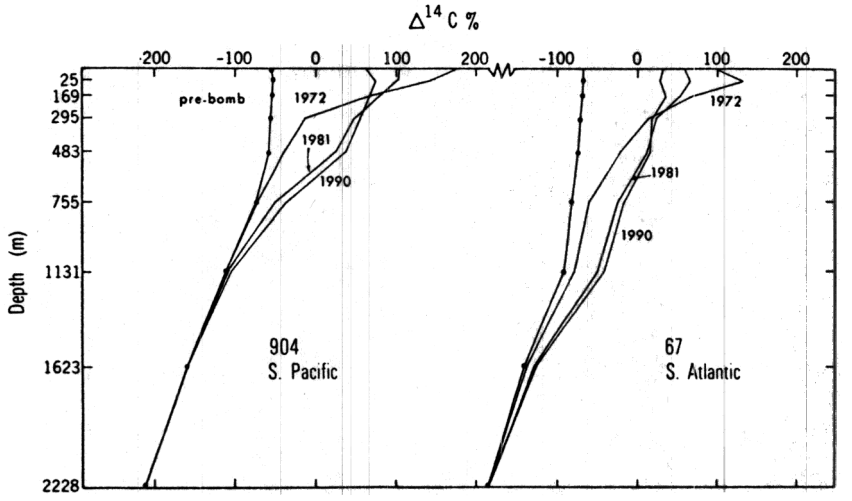

Fig. 14. Predicted vertical profiles of $\Delta^{14}C$ at locations on either side of the tip of South America representing the prebomb equilibrium and 1972, 1981, and 1990 in the P model. Station 904 is located in the Pacific, and station 67 is in the Atlantic. Locations are plotted in Figure 12.

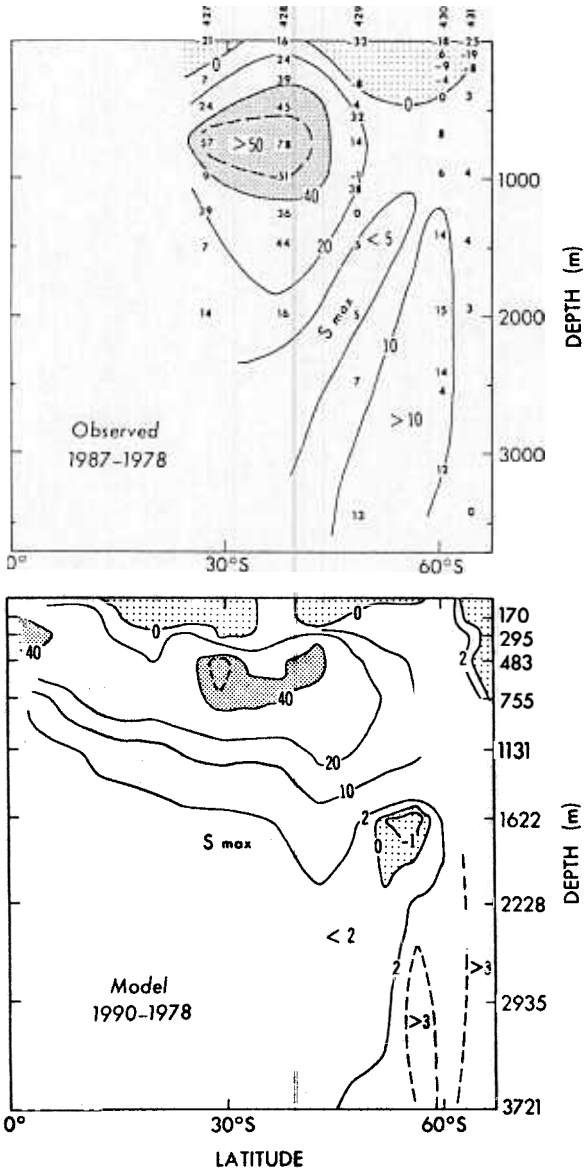

Fig. 15. Comparison of (top) observed and (bottom) modeled ^{14}C changes along the western Indian Ocean GEOSECS track (see Figure 12) between 1978 and the late 1980s. Calculation of observed changes were made by linearly interpolating GEOSECS observations (1978) to the depths where ^{14}C samples were collected during the INDIGO expedition (1985–1987 [*Ostlund and Grall*, 1988]). Results of the interpolation and differencing are indicated by the small numbers at INDIGO sample depths. GEOSECS station numbers are given at top. Corresponding INDIGO stations are, from north to south, 3, 7, 103/11, 76, and 79.

Figure 14 shows a series of vertical ^{14}C profiles sampled from the model over time at two locations, one from the Pacific side of South America (904), the other from the Atlantic side (67). For station locations, see Figure 12. There is a large increase in bomb ^{14}C inventory at station 904 between 300 and 750 m (levels 4–6) between 1972 and 1981. At the Atlantic station 67 this same inventory increase is seen to extend down to 1500 m. The profiles at station 67 sample the same pool of bomb ^{14}C seen at station 904, but the bomb ^{14}C inventory at station 67 is pushed downward after the eastward flowing water mass comes through the Drake Passage.

In summary, the convecting water mass in the western South Pacific flows across the Pacific to the vicinity of South America, where part of it is pushed downward and moves northward into the South Pacific. The remainder moves through the Drake Passage and is pushed down again on the Atlantic side and continues moving to the east. In Figure 11 one sees a tongue of this water bending back to the north and west in the eastern South Atlantic. This water penetrates far into the South Atlantic, eventually flowing equatorward along the margin of South America. The downward penetration and northward spreading illustrated by Figures 11, 13, and 14 represents the model's major ventilation pathway for levels 5, 6, and 7 (500–1100 m) in the southern hemisphere. As we will show in the Discussion section, the *T-S* properties of this water mass depart widely from observed *T-S* relationships. Because of the similarities with Subantarctic Mode Water, we conclude that the mechanisms by which this water mass forms are realistic. The problem mainly seems to be that the convection which produces these features occurs in the wrong places.

Deep Penetration of Bomb ^{14}C in the Circumpolar Region

In this section we examine the post-GEOSECS penetration of bomb ^{14}C into the deeper levels of the circumpolar region. More specifically, we attempt to assess how the model's circumpolar overturning cell, which figures prominently in the discussion of part 1, influences the deep penetration of bomb ^{14}C. The model's circumpolar overturning viewed in a zonally integrated meridional section (top panel of Figure 4, part 1) features 10–15 Sverdrups of downward flow to 3000–3500 m between 35° and 55°S and upward flow between 55° and 65°S. The deep upwelling in the model creates a strong front in radiocarbon concentrations separating the very "old" water of the deep Pacific and the "young" water of the Atlantic from the intermediate-aged water around Antarctica. In order to relate the motions of the model circumpolar cell to the time scales of the bomb transient we note that 200–300 years are required to flush the volume of circumpolar water via the circumpolar overturning. In contrast, about 30 years are required for a water parcel at 2000 m to circumnavigate the globe in the circumpolar current.

Figure 15 shows a comparison between the observations and the model of the bomb ^{14}C penetration across the circumpolar region in the western Indian Ocean during the 1980s. The top panel shows the change in ^{14}C content between 1978, as measured by GEOSECS, and during 1985–1987 as measured by INDIGO [*Ostlund and Grall*, 1988]. The bottom panel shows the change in ^{14}C content in the model between 1978 and 1990.

The observations show a strong increase in ^{14}C levels between 30°S and 40°S centered between 500 and 1000 m. This water mass has salinities intermediate between high-salinity subtropical water near the surface and low-salinity Antarctic Intermediate Water below. In its *T-S* properties it coincides with Subantarctic Mode Water formed in the eastern Indian Ocean [*McCartney*, 1977]. There is a distinct minimum in bomb ^{14}C content below 1000 m near 45°S which coincides with a local salinity maximum associated with the outflow of North Atlantic Deep Water (NADW). An additional bomb ^{14}C maximum with increases of more than 10‰ appears below and to the south of the NADW minimum.

This deeper maximum is associated with lower salinities and high silica concentrations. It appears to represent the same water mass labeled with significant amounts of F-11 in the AJAX section down the prime meridian in the eastern South Atlantic (R. F. Weiss et al., personal communication (1988); these unpublished results have been reproduced by *Sarmiento* [1988]). The low salinity, low temperature, and high silica content of this water attest to an origin in the Weddell Sea [*Weiss et al.*, 1979] followed by extensive contact with silicious bottom sediments during an eastward traverse [see *Edmond et al.*, 1979].

Perhaps the most notable feature of the observations down the western Indian GEOSECS track is the fact that virtually all of the water south of 40°S, with the exception of the near-surface waters, has picked up some bomb ^{14}C between 1978 and 1987. The deep sampling density of the INDIGO stations unfortunately leaves some of the deep water unsampled. The F-11 data in the eastern Atlantic, however, lead to a similar conclusion: almost all the deep water in the Atlantic and Indian ocean sectors of the circumpolar region is ventilated to some degree over a 25-year time scale.

The bottom panel of Figure 15 shows the model producing a Subantarctic Mode Water bomb ^{14}C maximum in approximately the right position. The deep penetration in the model, however, does not replicate what is seen in the observations. The 20‰ isoline extends nearly to 2000 m in the observations but only to 1200 m in the model. A "wedge" of low bomb ^{14}C concentrations, defined by the 2‰ contour near 40°S, extends below 2000 m. The bomb ^{14}C in the "2‰ wedge" can be traced back upstream to a deep increase in bomb ^{14}C seen just east of South America in Figure 14. Adjacent to the 2‰ wedge on the left near 30°S is the model's salinity maximum of North Atlantic origin. The model's salinity maximum is located too far to the north and has yet to pick up any bomb ^{14}C. Adjacent to the 2‰ wedge on the right near 55°S is a minimum in prebomb ^{14}C. The ^{14}C minimum labels this water as a slug of Pacific water which has come through the Drake Passage. This water mass has not picked up any bomb ^{14}C either. In fact, model ^{14}C concentrations are drifting downward, producing negative contours when the 1990–1978 difference is computed. Figure 15 shows small bomb ^{14}C increases in the model at depth adjacent to Antarctica which are not nearly as large as the observed increases.

Given what we said at the beginning of this section regarding the time scales of ventilation attributable to the circumpolar overturning cell, one would not expect much bomb ^{14}C to penetrate to depth in this area via the overturning cell alone. Indeed, the correlations between observed bomb ^{14}C features in Figure 15 with water mass structures demonstrate that much of the deep bomb ^{14}C penetration in the circumpolar region occurs via the major thermohaline components of the circulation, i.e., the North Atlantic Deep Water and Antarctic Bottom Water. It is obvious from Figure 15 that one of the model's major faults is its inability to adequately ventilate its deep circumpolar region by these mechanisms over the time scales of the bomb ^{14}C transient.

Bomb ^{14}C in the North Atlantic

Figure 16 shows a series of model snapshots of bomb ^{14}C in the North Atlantic at level 8 (1622 m) for the years 1972, 1981, and 1990. Also shown in Figure 16 are the velocity vectors for the model's horizontal circulation at level 8. As we pointed out in part 1, the model's version of North Atlantic Deep Water is confined to levels 8 (1622 m) and 9 (2228 m). It cannot penetrate any deeper because it is less dense than water of Antarctic origin which has spread into the North Atlantic in the deeper levels 11 and 12. The model generates a boundary current in levels 8 and 9 which carries its NADW to the south and eventually connects up with the circumpolar current. The boundary current can easily be traced by the velocity vectors and the −70 and −80 ^{14}C isolines in Figure 16.

Most of the model's bomb ^{14}C uptake in the northern Atlantic occurs in the eastern Norwegian Sea, where the model convects to the bottom. There is a strong flow of water to the west in level 7 carrying water of Norwegian Sea origin across the sill connecting Europe and Greenland. More convection and sinking occur south of Greenland, carrying bomb ^{14}C down to levels 8 and 9. This is the origin of the bomb ^{14}C seen in the top panel of Figure 16. Once in the North Atlantic the bomb ^{14}C becomes caught up in the model's cyclonic subpolar gyre. It spreads first to the south and then to the east along 45°N. The flow then turns to the south off Europe and flows to the west across the Atlantic. By 1990 a rather strong front in ^{14}C has developed between 30°N and 40°N as the continued southward spreading is limited by the flow boundary. When the westward flow reaches North America, it turns south again as the deep boundary current. The boundary current at 25°N in the model is only showing the first signs of bomb ^{14}C by 1990. The Transient Tracers in the Ocean (TTO) observations show small amounts of tritium in the boundary current off the Bahamas by 1981 [*Ostlund and Grall*, 1987], nearly 10 years before bomb ^{14}C reaches this area in the model. Chlorofluorocarbon observations show F-11 in the boundary current reaching the equator by 1983 [*Weiss et al.*, 1985].

Figure 17 displays a series of vertical profiles from the model and the observations at the location of GEOSECS 27 (42°N). GEOSECS 27 was reoccupied as TTO 228 in 1981. The observations show an almost uniform increase in bomb ^{14}C between 1972 and 1981 of about 20‰ which extends between 1000 m and the bottom (4800 m). There is a zone between 700 m and 1000 m in which no increase is observed. The model predicts a small increase by 1981 between 800 m and 2500 m and a more substantial increase by 1990. A reoccupation of GEOSECS 29 at 36°N, 600 km to the south, by the TTO test cruise station 4 in 1980 shows no increase in ^{14}C below 1000 m between 1972 and 1980 [*Ostlund and Grall*, 1987]. TTO tritium measurements below 2000 m also show a drop-off in tritium values south of 40°N [*Ostlund and Grall*, 1987]. It is very evident in Figure 17 that the model's North Atlantic ventilation does not extend deep enough and does not transport bomb ^{14}C into the interior fast enough.

The strong midbasin front in the southward penetration of bomb ^{14}C at level 8 in the North Atlantic is consistent with potential vorticity patterns observed on isopycnal surfaces at shallower depths [*Keffer*, 1985]. Keffer shows that the North Atlantic has a relatively uniform potential vorticity region on the isopycnal surface $\sigma_\theta = 27.40$ (~900 m) in the eastern half of the basin north of 30°N, indicating strong ventilation. This area of uniform potential vorticity is bounded to the south by a stagnant area of closed east-west oriented geostrophic contours. The ventilated thermocline model of *Luyten et al.* [1983] provides an explanation of this boundary between a region of active circulation and a

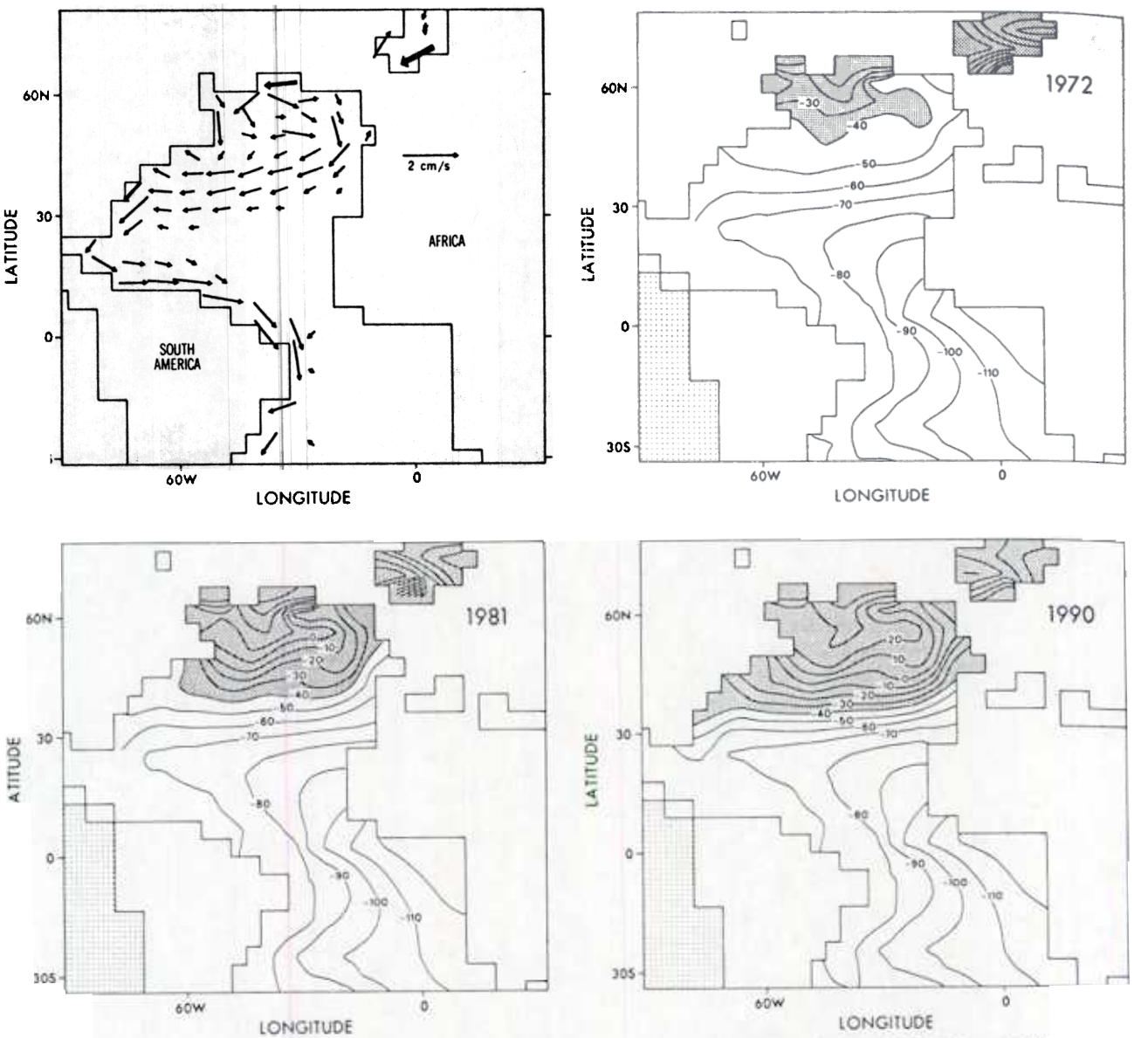

Fig. 16. Snapshots of the predicted $\Delta^{14}C$ in the North Atlantic at level 8 (1622 m) during 1972, 1981, and 1990 showing the invasion of bomb ^{14}C in the depth range of the North Atlantic Deep Water in the P model. Also shown are the model's current vectors at this depth. Carbon 14 values in excess of −40‰ are shaded with heavy stippling.

shadow region of weak circulation. The model of Luyten et al. also explains why the shadow region extends further north at greater depth.

Discussion

Water Mass Relationships in the Circumpolar Region

The model shows that the circumpolar current region is the site of an important downward pathway in the second decade of bomb ^{14}C entry to the ocean (Figures 9 and 11). On the other hand, the model does not produce a good simulation of the low-salinity intermediate water masses of the southern hemisphere, which are a major feature of the observed water mass structure in this region.

Temperature-salinity profiles at three points along the northern edge of the circumpolar region are shown in Figure 18. Figure 18*a* shows results from the P model, Figure 18*b* shows observed profiles from the same locations taken from an interpolation of data from *Levitus* [1982] to the model grid, and Figure 18*c* shows results from a higher-resolution, seasonally forced model by *Bryan and Lewis* [1979]. Station locations are given in Figure 12. Station 435 is located in the Indian Ocean, just west of Australia at 40°S. Station 904 is located downstream off the tip of South America at 47°S. Station 68 is located around the other side of the Drake Passage in the South Atlantic at about the same latitude. In Figure 18*a* we show in addition the *T-S* properties of the convecting water mass in the P model at station 911 south of Australia.

Water mass properties in the upper 500 m become progressively colder and fresher along the north side of the circumpolar current as it moves from the Indian Ocean across the Pacific, and around South America to the Atlantic

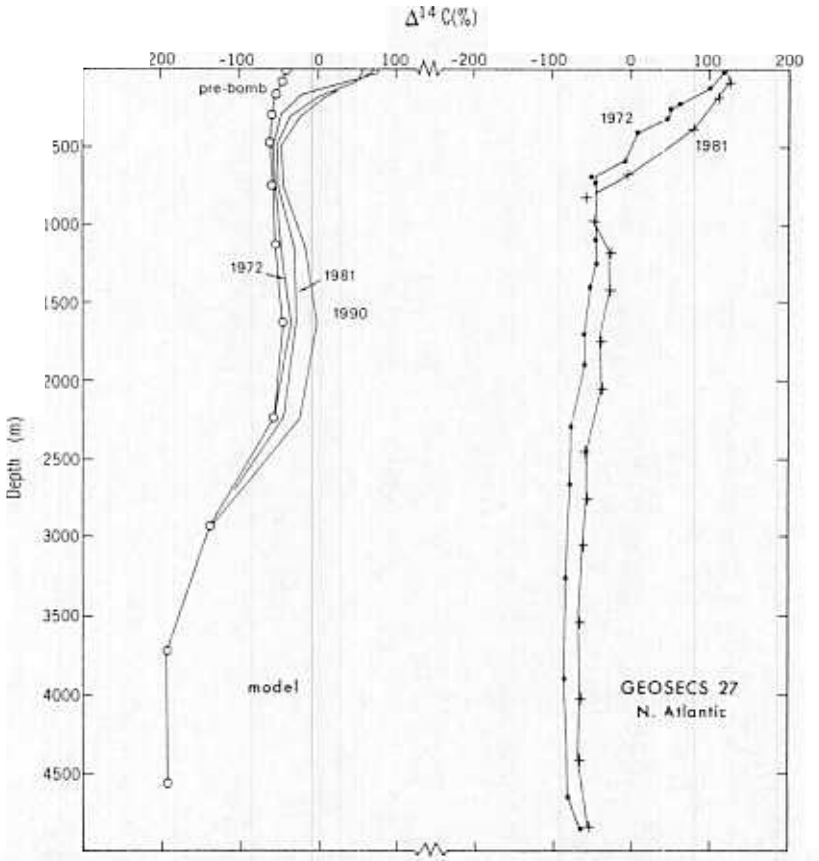

Fig. 17. Comparison between model predictions and observations of vertical profiles of bomb ^{14}C at the location of GEOSECS 27 in the North Atlantic. (Left) Results of the P model are given for the prebomb equilibrium, 1972, 1981, and 1990. (Right) Data are shown for 1972 (GEOSECS 27; solid circles) and 1981 (TTO station 228; pluses [*Ostlund and Grall*, 1987]).

(Figure 18*b*). *McCartney* [1977] documented the existence of very deep winter mixed layers in the Indian and Pacific sectors which give rise to the Subantarctic Mode Waters along the northern edge of the circumpolar current. We have plotted the *T-S* properties of the mixed layers at the eastern and western extremes of McCartney's transect in the three panels of Figure 18 as the triangles labeled AB160 and E192. Locations are given in Figure 12. McCartney attributed the east to west tendency in the *T-S* properties to the formation of mode water at progressively higher latitudes as the circumpolar current shifts southward as it moves from the Indian Ocean to the Drake Passage.

The *T-S* properties of the upper 750 m at stations 435 and 911 in the P model are not dissimilar to the warm and salty extreme of McCartney's mixed layers. There is no evidence, however, that McCartney's cold and fresh surface properties penetrate much below the surface anywhere. Model surface waters are constrained by the boundary conditions to become fresher and colder along the axis of the current, but the water column at station 904 in the eastern South Pacific is not stirred enough to overcome the local stratification. As a result, a salinity maximum exists between 300 and 800 m which carries the signature of the high salinity waters off Australia. The same *T-S* signature extends around South America into the Atlantic.

Two factors are probably contributing to the failure of the P model to form a low-salinity, intermediate depth water mass. First, the P model produces deep convection at lower latitudes than is observed. Figure 16 in part 1 documents the model's deep convection near the perimeter of Australia between 35° and 40°S. The deep winter mixed layers documented by McCartney were observed between 43° and 52°S in this sector. Second, the P model lacks the effect of seasonal changes in the wind and surface water properties. The model may be missing possible correlations between Ekman pumping, wintertime convection, and forced convection essential for forming South Pacific mode waters. As evidence for this, Figure 18*c* shows the *T-S* properties from another model similar to the P model which includes seasonal variations in its boundary conditions [*Bryan and Lewis*, 1979]. The agreement with observations is much improved. The Bryan and Lewis model is constructed from a 2° grid (versus ~4° here) and includes an enhancement of local vertical mixing due to wind stirring [*Kraus and Turner*, 1967].

A third factor contributing to the P model's failure to form a low-salinity mode water in the South Pacific is the fact that the P model's Drake Passage is much wider than the Drake Passage in the real ocean. Figure 2 in part 1 illustrates the difference. South America extends down to 50° in the P model, versus 55° in the real ocean. The position of the circumpolar current is strongly influenced by the position of the Drake Passage. The latitudes where the Subantarctic Mode Waters form appear to be strongly influenced by the northern boundary of the circumpolar current. Since surface water at 55° is colder and more dense than surface water at 50°, surface water near the tip of South America in the model is not as cold and dense as it should be. Indeed, Figures 18*a*

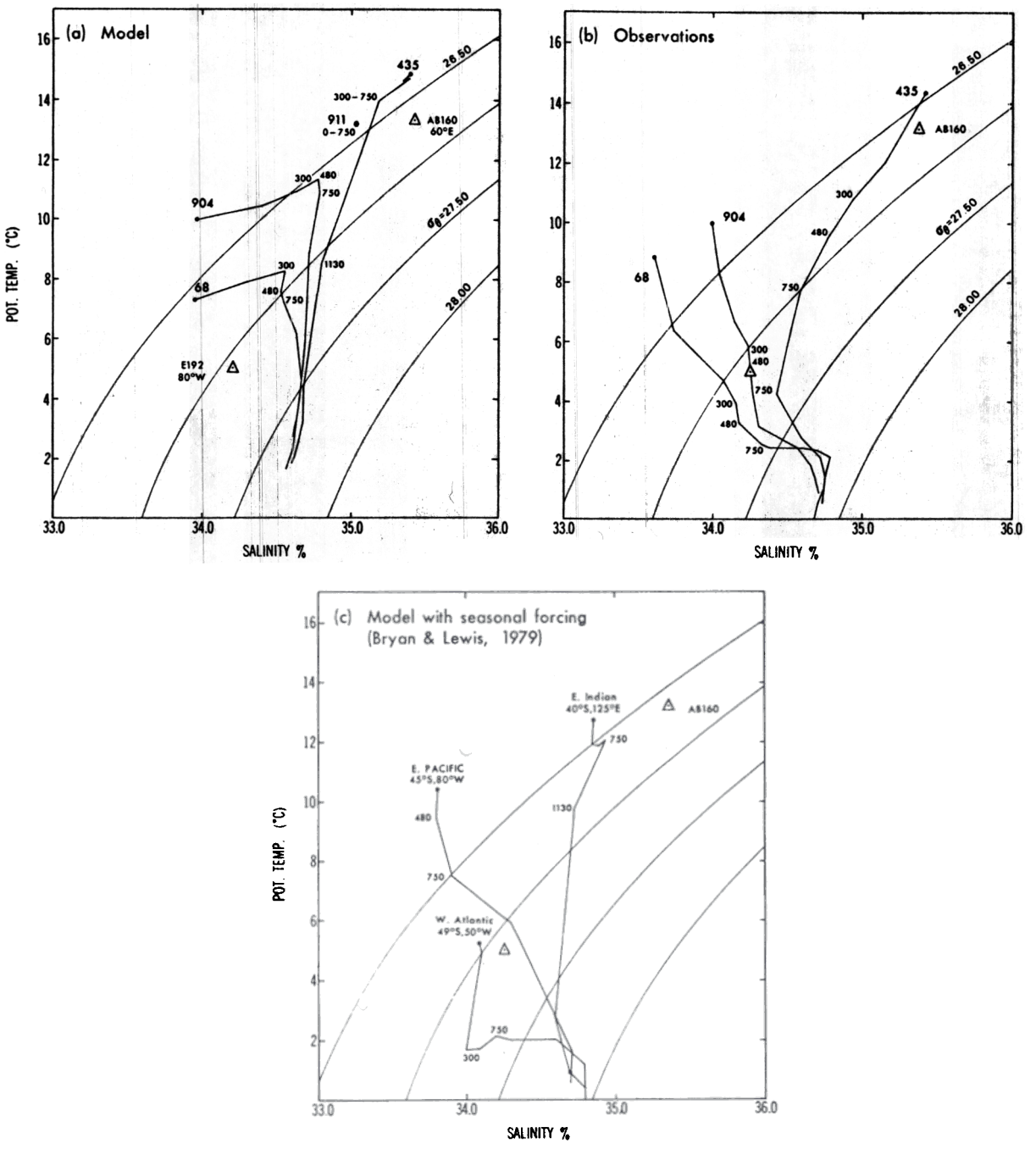

Fig. 18. Comparison between water mass properties in the circumpolar region in the observations and two different models. Plots show profiles of potential temperature and salinity at station locations 435 (Indian), 904 (eastern South Pacific), and 68 (South Atlantic). Results from the P model are shown in Figure 18*a*. Observations in Figure 18*b* have been interpolated from the data set of *Levitus* [1982] to the model grid. Results from the model of *Bryan and Lewis* [1979] are shown in Figure 18*c* at slightly different locations.

and 18*b* show that both observed and model surface waters at station 904 are less dense than the surface waters at the northern edge of the circumpolar current south of Australia. If the tip of South America were 5° further south in the model the surface waters near the tip of South America would be 0.5‰ more dense. The *Bryan and Lewis* [1979] model is able to incorporate a more realistic Drake Passage configuration because of its higher spatial resolution.

We conclude that although the model fails to properly simulate the formation of low-salinity intermediate waters in the circumpolar region, the model does form intermediate depth water masses by realistic mechanisms. The model forms its intermediate depth water masses about 5° too far north and concentrates its deep convection in a single sector of the circumpolar belt.

Spurious Upwelling Along Western Boundary Currents

Lateral mixing in the model is oriented along horizontal surfaces in the model, whereas a more accurate description

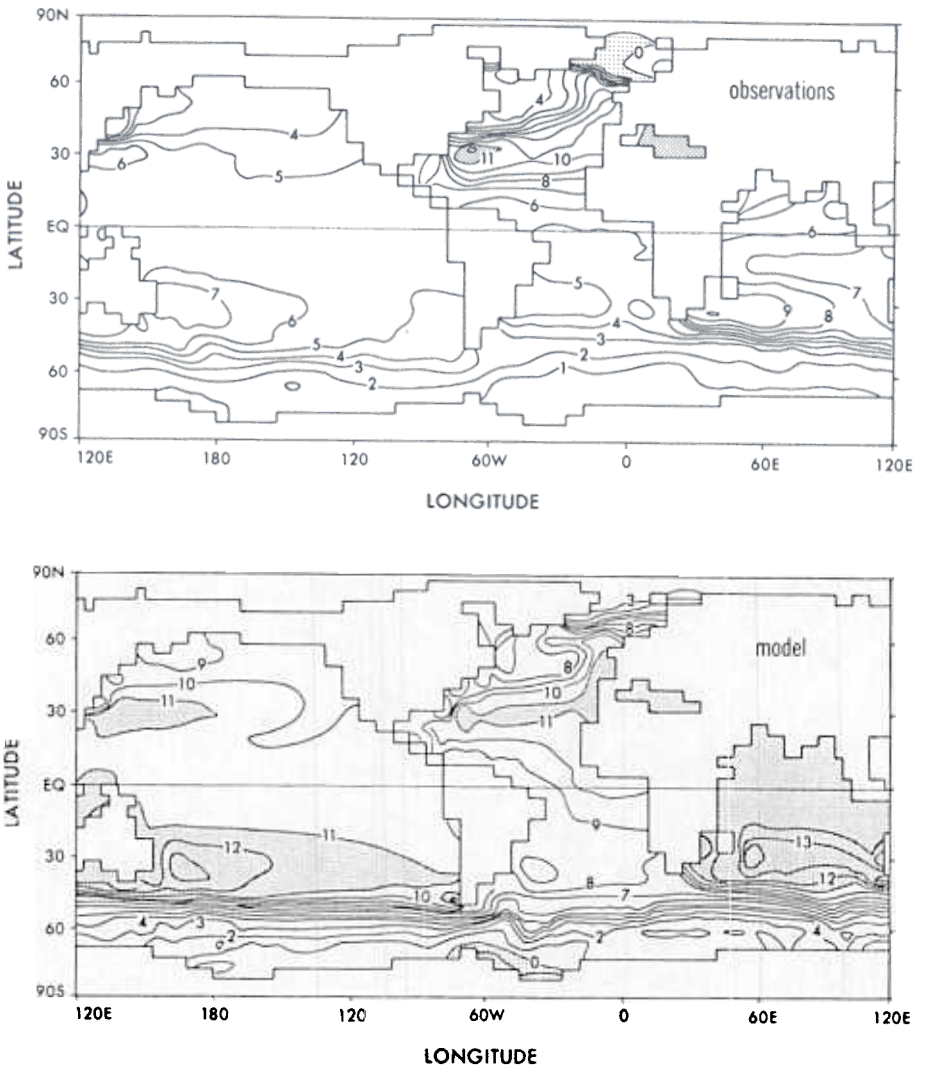

Fig. 19. Comparison of potential temperatures at the depth of model level 6 (755 m) between (top) observations and (bottom) the P model. Observed temperatures have been interpolated from the *Levitus* [1982] data set to the model grid.

of lateral mixing is a spreading along surfaces of constant density [*McDougall and Church*, 1986]. In the presence of strong western boundary currents, density surfaces slope upward sharply near the ocean's margin. The purely horizontal mixing of the model thus tends to flatten the density structure and transport a great deal of heat across the current. *Veronis* [1975] pointed out that the horizontal mixing in primitive equation models produced an artificial upwelling of water inshore of western boundary currents, as water upwelled from depth to balance the spurious flux of heat.

In Figure 7 we showed that this artificial upwelling, and the eastward spreading of the upwelled water mass, produced a glaring deficit in the predicted bomb ^{14}C inventory off North America and, to a lesser degree, in the South Atlantic and North and South Pacific. Tracing the changing inventories of bomb ^{14}C over time (Figures 8 and 9) indicates that the water which upwells inshore of the Gulf Stream eventually picks up bomb ^{14}C such that the deficit is gradually erased. Analysis of the model's circulation reveals that this upwelled water is derived from water flowing out of the Norwegian Sea. About one third of the model's North Atlantic Deep Water production returns to the surface through the upwelling inshore of the Gulf Stream. This is clearly unacceptable and must be improved in future models.

Correspondence Between the Density Field and Ventilation

As pointed out in the introduction to part 1, coarse-resolution, primitive equation models of this type have certain well known deficiencies as regards the density structure. Model temperatures in the thermocline are significantly warmer than observed temperatures. Model temperatures deviate most strongly in levels 5 through 8, roughly 500–1500 m (see Table 2 of part 1). Thus a typical temperature profile in low and middle latitudes has too little of the characteristic curvature seen in observed profiles. Figure 19 shows a comparison of the observed temperature field in the ocean with that of the model at 755 m (level 6). Model temperatures are typically 4°–5°C warmer than observed temperatures.

Deviations approaching 6°C occur in the far North Pacific, eastern Indian Ocean, and subtropical South Pacific. Had this model been forced with seasonal boundary conditions instead of annual mean conditions there would be some improvement, but not enough to account for these differences [*Levitus*, 1987].

Although this is a fairly subjective judgement, we would argue on the basis of these radiocarbon studies, that the GFDL ocean model does a better job of simulating the ventilation of the ocean's interior than it does of simulating the ocean's density and water mass structures. Why should this be so? One possible answer to this question is that the water ventilating the interior has the correct radiocarbon content but is too warm. When vertical mixing is too large a term in the temperature balance, the downward mixing of 25° water in low latitudes warms the thermocline. The radiocarbon content of this water, however, is not much different from that of 15° water in higher latitudes. Thus the vertical radiocarbon balance could appear to be correct while the temperature balance is obviously not. The fact that lateral mixing is oriented along horizontal surfaces in the model, rather than along density surfaces which slope upward toward the poles, does not help. More vigorous mixing where surface waters are cool (5°–15°) and less mixing where surface waters are warm should improve the temperature simulation without dramatically changing the radiocarbon balance.

One factor which may prove very important in this regard is the inability of the model to produce Subantarctic Mode Waters in the correct places. Figure 11 shows that level 6 is ventilated quite readily with bomb ^{14}C in all three ocean basins. We showed above that the temperature of the water associated with this ventilation was 13°–14°C at its points of origin in the model. The observed temperature of mode water forming in the eastern Pacific is about 5°C. Given the time scale over which level 6 is ventilated in all three southern hemisphere ocean basins in the model, it is apparent that much of the excess heat in the thermoclines of all three southern hemisphere ocean basins comes in via the model's warm Subantarctic Mode Water.

Relevance of Bomb Radiocarbon to Global Environmental Perturbations

The ocean is currently absorbing anthropogenic releases of fossil and biospheric CO_2 as well as tropospheric heat generated by this excess CO_2 and the other so-called "greenhouse" gases. However, the measurement precision for CO_2 in seawater is only now, in the 1980s, good enough to detect anthropogenic changes. No global survey of oceanic CO_2 using the current technology has been made to establish a baseline against which future changes can be compared. Warming of the ocean damps tropospheric temperature changes caused by the greenhouse gases [*Hansen et al.*, 1985], but strong seasonal and interannual variability in ocean temperatures preclude documentation of current anthropogenic effects. Our ability to assess the current oceanic uptake of CO_2 and greenhouse heat and to predict future uptake therefore rests largely on the ability of ocean models like this one to accurately simulate the penetration of these substances into the ocean's interior. The relevance of making bomb ^{14}C measurements and simulating the penetration of bomb ^{14}C in an ocean model derives from the straightforward global-scale validation that these exercises afford the model calculation.

Inputs of heat and CO_2 to the ocean are governed by gradually accelerating increases in atmospheric concentrations of CO_2 and the other greenhouse gases. Inputs of bomb radiocarbon over the last 40 years have been governed by atmospheric ^{14}C concentrations which peaked sharply in the early 1960s and have since declined (Figure 1). Because of the different input histories and the much longer time scale for surface water ^{14}C equilibration [*Broecker and Peng*, 1974], bomb ^{14}C is not an exact analog for the uptake of heat and CO_2.

The release of fossil fuel CO_2 to the atmosphere has a characteristic rate of increase of about 30 years [*Oeschger et al.*, 1975]. The 30-year time scale determines the volume of ocean water which is available for taking up the excess CO_2 and heat from the atmosphere [*Broecker et al.*, 1979]. The shallow volume of ocean in which bomb ^{14}C concentrations rose most strongly in the first decade after the bomb tests will remain largely saturated with excess CO_2 on the 30-year time scale. These layers will absorb a significant, but limited, share of anthropogenic releases. The huge volume of water in the deep ocean will not take up an appreciable amount of CO_2 on this time scale. On the other hand, the layers of ocean just witnessing a build-up of bomb ^{14}C 15–50 years after the bomb tests are the layers for which the model validation is most critical. Model flaws affecting the layers of the ocean ventilated on time scales commensurate with the CO_2 release will produce the most significant errors in model predictions.

In this paper we have demonstrated that the GFDL model predicts a pattern of bomb ^{14}C input and inventory accumulation that is significantly different for the years following the GEOSECS survey than for the years preceding GEOSECS. The GEOSECS surveys were completed less than 15 years after the peak in atmospheric ^{14}C concentrations. We would argue that the water masses associated with significant bomb ^{14}C penetration after GEOSECS, i.e., the deep North Atlantic, the southern hemisphere thermocline, and the circumpolar region, are the critical regions of the ocean for monitoring future bomb ^{14}C changes. Flaws in ocean circulation models affecting these water masses deserve special attention.

The volumes of ocean witnessing a build up of bomb ^{14}C after GEOSECS are being tagged with atmospheric bomb ^{14}C at much lower concentrations than during the 1960s and early 1970s. It is not easy to identify what part of the observed ^{14}C concentration is bomb derived and what part is natural. One must make measurements at two points in time to identify the bomb ^{14}C. In the few places where we have been able to make these comparisons between the model and the observations (Figures 13, 15, and 17) we find that the model reproduces important features but still leaves a great deal of room for improvement.

An important caveat must be included relating to mesoscale eddies. An implicit assumption in this study is that the downward spreading of ^{14}C is mainly controlled by large-scale advection and convection and that the transport of tracers by mesoscale eddies can be represented by the addition of a simple, low level horizontal mixing. While this approach appears justified in analyzing the GEOSECS data set, which can only resolve very large scale global features, it is not generally applicable where more detailed features must be resolved. This is demonstrated in a very clear way

by *Cox* [1985], who compares idealized tracer simulations with eddy and non-eddy resolving models.

SUMMARY AND CONCLUSIONS

The ^{14}C measurements of the GEOSECS program represent a unique oceanographic resource. No other tracer combines information related to both the very long time scales of the deep ocean and the shorter time scales of thermocline ventilation. No other anthropogenic tracer can match both the global signal and global data coverage of bomb ^{14}C. A detailed comparison of the predicted invasion of the ocean by bomb-produced ^{14}C and the ground truth of the GEOSECS measurements provides a stringent test of the ability of an ocean model.

The analysis in this paper has revealed a number of flaws in the GFDL ocean model which are pertinent to problems related to ocean ventilation. The model's calculated inventory of bomb ^{14}C at the time of GEOSECS surveys is low by about 16%. We have concluded that low model gas exchange rates are responsible. The P model's gas exchange rates are on average 20% or so below the global mean values suggested by box models. The model's upper ocean vertical mixing, particularly in the recirculation regions of its subtropical gyres and in the cooler temperate and subpolar areas, also appears to be too weak. The tendency of this model to produce upwelling inshore of western boundary currents produces glaring deficiencies in the model's bomb ^{14}C inventory distribution. The model successfully accounts for the pre-GEOSECS shift in bomb ^{14}C inventories from the equatorial to subtropical areas but appears, in the Pacific at least, to make this transfer too slowly, as is documented by comparisons with coral records. The model also moves bomb ^{14}C into the interior of the deep North Atlantic and deep circumpolar region much too slowly.

One of the most interesting insights gained from the model analysis is that the pattern of bomb uptake in the decade following GEOSECS should be quite different from that in the decade preceding GEOSECS. Although such a finding is not surprising in principle, the model makes some detailed three-dimensional predictions about where the inventory accumulation should be occurring. Much of the inventory accumulation post-GEOSECS is predicted to be below 1000 m in the North Atlantic, in the southern hemisphere thermocline, and in the circumpolar region. The TTO observations have already documented the North Atlantic ^{14}C buildup. But the model's predictions regarding the southern hemisphere buildup and the distinction between thermoclines in the northern and southern hemispheres of the Pacific and Indian Oceans have been largely unanticipated and largely untested by ocean surveys. The model highlights the important role of Subantarctic Mode Waters forming along the northern edge of the circumpolar current. The model fails to form mode waters in the right places or with the observed *T-S* properties, but it does reproduce the convection, weak stratification, and northward lateral spreading characteristic of observed mode waters.

In their analysis of the GEOSECS ^{14}C observations, BPOS argued that the redistribution of bomb ^{14}C from areas where it entered the ocean to areas where it was eventually detected posed a strong constraint on models of global ocean circulation. We have found that the GFDL model reproduces most of the features documented by BPOS at the time of GEOSECS. With the benefit of hindsight we can say that this result is not surprising. Bomb ^{14}C uptake and transports by the ocean during the first decade after the bomb tests are dominated by a huge and nearly uniform atmospheric input and the wind-driven circulation of the upper ocean. These processes are strongly constrained by boundary conditions (like gas exchange and wind stresses) which are largely independent of the model itself. Once longer time scales are considered, however, processes involving water mass transformation (like deep convection, Subantarctic Mode Water formation, and deep water formation) become important. These processes are, for the most part, not beginning to affect bomb radiocarbon inventories at the time of GEOSECS. They are intrinsically more subtle and more difficult to simulate in a model. Comparisons with the limited data available for the post-GEOSECS years yields a rather tenuous passing grade for model performance.

In the introduction to part 1 we remarked on the fact that the version of the model used in this study is a simplified general circulation model which has few of the embellishments which have been suggested or previously tested to improve its fit to observed temperature and salinity distributions. We have now attempted to validate the model against a rich data set which has heretofore been only barely exploited for its model validation potential. The model reproduces many of the features of these data quite well, but there is clearly much room for improvement. Many of the model flaws which have been identified in the bomb ^{14}C study have not been recognized before. Some of the flaws are relatively trivial to correct; others will require more substantial efforts. Armed with new insights and a new validation tool we can push ahead toward an improved ocean circulation model.

Acknowledgments. The authors would like to acknowledge internal reviews by J. Sarmiento, S. Manabe, and G. Shaffer. Special thanks are also due Wendy Marshall, Phil Tunison, Jeff Varanyak, and Cathy Raphael for their assistance in preparing the manuscript and figures. This project was initiated while the first author was supported by the Carbon Dioxide Research Division, U.S. Department of Energy, under contract DE-AC05-840R21400 with Martin Marietta Systems, Inc. (subcontract 19X-27405C with Princeton University).

REFERENCES

Bard, E., M. Arnold, H. G. Ostlund, P. Maurice, P. Monfray, and J.-C. Duplessey, Penetration of bomb radiocarbon in the tropical Indian Ocean measured by means of accelerator mass spectrometry, *Earth Planet. Sci. Lett.*, *87*, 379–389, 1988.

Bard, E., M. Arnold, J. R. Toggweiler, P. Maurice, and J.-C. Duplessey, Bomb ^{14}C in the Indian Ocean measured by accelerator mass spectrometry: Oceanographic implications, *Radiocarbon*, in press, 1989.

Broecker, W. S., and T. H. Peng, Gas exchange rates between air and sea, *Tellus*, *26*, 21–35, 1974.

Broecker, W. S., and T.-H. Peng, The distribution of bomb-produced tritium and radiocarbon at GEOSECS station 347 in the eastern North Pacific, *Earth Planet. Sci. Lett.*, *49*, 453–462, 1980.

Broecker, W. S., and T.-H. Peng, *Tracers in the Sea*, Lamont-Doherty Geological Observatory, Palisades, N. Y., 1982.

Broecker, W. S., T. Takahashi, H. J. Simpson, and T.-H. Peng, Fate of fossil fuel carbon dioxide and the global carbon budget, *Science*, *206*, 409–418, 1979.

Broecker, W. S., T.-H. Peng, and R. Engh, Modeling the carbon system, *Radiocarbon*, *22*, 565–598, 1980.

Broecker, W. S., T. -H. Peng, H. G. Ostlund, and M. Stuiver, The distribution of bomb radiocarbon in the ocean, *J. Geophys. Res.*, *90*, 6953–6970, 1985.

Bryan, K., A numerical method for the study of the circulation of the world ocean, *J. Comput. Phys.*, *4*(3), 347–376, 1969.

Bryan, K., and L. J. Lewis, A water mass model of the World Ocean circulation, *J. Geophys. Res.*, *84*, 2503–2517, 1979.

Cox, M. D., An eddy resolving numerical model of the ventilated thermocline, *J. Phys. Oceanogr.*, *15*, 1312–1324, 1985.

Craig, H., The natural distribution of radiocarbon and the exchange time of carbon dioxide between atmosphere and sea, *Tellus*, *9*, 1–17, 1957.

Druffel, E. M., Bomb radiocarbon in the Pacific: Annual and seasonal timescale variations, *J. Mar. Res.*, *45*, 667–698, 1987.

Edmond, J. M., S. S. Jacobs, A. L. Gordon, A. M. Mantyla, and R. F. Weiss, Water column anomalies in dissolved silica over opaline pelagic sediments and the origin of the deep silica maximum, *J. Geophys. Res.*, *84*, 7809–7826, 1979.

Esbensen, S. K., and Y. Kushnir, The heat budget of the global ocean: An atlas based on estimates from surface marine observations, *Rep. 29, Clim. Res. Inst.*, Oreg. State Univ., Corvallis, 1981.

Fine, R. A., J. L. Reid, and H. G. Ostlund, Circulation of tritium in the Pacific Ocean, *J. Phys. Oceanogr.*, *11*, 3–14, 1981.

Hansen, J., G. Russell, A. Lacis, I. Fung, and D. Rind, Climate response times: Dependence on climate sensitivity and ocean mixing, *Science*, *229*, 857–859, 1985.

Hellerman, S., and M. Rosenstein, Normal monthly wind stress over the world ocean with error estimates. *J. Phys. Oceanogr.*, *13*, 1093–1104, 1983.

Holland, W. R., Ocean tracer distributions, *Tellus*, *23*, 371–392, 1971.

Keffer, T., The ventilation of the world's oceans, Maps of the potential vorticity field, *J. Phys. Oceanogr.*, *15*, 509–523, 1985.

Konishi, K., T. Tanaka, and M. Sakanoue, Secular variations of radiocarbon concentration in sea water: Sclerochronological approach, in *Proceedings of the Fourth International Coral Reef Symposium, Manila*, vol. 1, edited by E. D. Gomez, pp. 181–185, Marine Science Center, University of the Philippines, 1982.

Kraus, E. B., and J. S. Turner, A one-dimensional model of the seasonal thermocline, II, The general theory and its consequences, *Tellus*, *19*, 98–106, 1967.

Levitus, S., Climatological atlas of the world ocean, *NOAA Prof. Pap. 13*, 173 pp., U. S. Government Printing Office, Washington D. C., 1982.

Levitus, S., A comparison of the annual cycle of two sea surface temperature climatologies of the world ocean, *J. Phys. Oceanogr.*, *17*, 197–214, 1987.

Luyten, J. R., J. Pedlosky, and H. Stommel, The ventilated thermocline, *J. Phys. Oceangr.*, *13*, 292–309, 1983.

Maier-Reimer, E., and K. Hasselmann, Transport and storage of CO_2 in the ocean—An inorganic ocean circulation carbon cycle model, *Clim. Dyn.*, *2*, 63–90, 1987.

McCartney, M. S., Subantarctic mode water, in: *A Voyage of Discovery*, edited by M. Angel, pp. 103–119, Pergamon, Elmsford, N. Y., 1977.

McCartney, M. S., The subtropical recirculation of mode waters, *J. Mar. Res.*, *40*, suppl., 427–464, 1982.

McDougall, T. J., and J. A. Church, Pitfalls with the numerical representation of isopycnal and diapycnal mixing, *J. Phys. Oceanogr.*, *16*, 196–199, 1986.

Oeschger, H., H. Siegenthaler, U. Schotterer, and A. Gugelmann, A box-diffusion model to study the carbon dioxide exchange in nature, *Tellus*, *27*, 168–192, 1975.

Ostlund, H. G., and C. Grall, TTO north and tropical Atlantic tritium and radiocarbon, *Data Rep. 16*, 227 pp., Tritium Lab., Rosenstiel Sch. of Mar. and Atmos. Sci., Univ. of Miami, Miami, Fla., 1987.

Ostlund, H. G., and C. Grall, INDIGO 1985–1987, Indian Ocean Radiocarbon, *Data Rep. 17*, 40 pp., Tritium Lab., Rosenstiel Sch. of Mar. and Atmos. Sci., Univ. of Miami, Miami, Fla., 1988.

Ostlund, H. G., and S. Niskin, Radiocarbon profile in the North Pacific 1969 GEOSECS intercalibration station, *J. Geophys. Res.*, *75*, 7667, 1970.

Quay, P. D., M. Stuiver, and W. S. Broecker, Upwelling rates for the equatorial Pacific Ocean derived from the bomb ^{14}C distribution, *J. Mar. Res.*, *41*, 769–792, 1983.

Reid, J. L., The shallow salinity minima of the Pacific Ocean, *Deep Sea Res.*, *20*, 51–68, 1973.

Sarmiento, J. L., A simulation of bomb tritium entry into the Atlantic Ocean, *J. Phys. Oceanogr.*, *13*, 1924–1939, 1983.

Sarmiento, J. L., A chemical tracer strategy for WOCE, *U. S. WOCE Plann. Rep. 10*, 181 pp., U. S. Plann. Off. for WOCE, College Station, Tex., 1988.

Swift, J. H., and K. P. Koltermann, The origin of Norwegian Sea Deep Water, *J. Geophys. Res.*, *93*, 3563–3569, 1988.

Toggweiler, J. R., A six zone regionalized model for bomb radiotracers and CO_2 in the upper kilometer of the Pacific Ocean, Ph.D thesis, Columbia Univ., New York, 1983.

Toggweiler, J. R., K. Dixon, and K. Bryan, Simulations of radiocarbon in a coarse-resolution world ocean model, 1, Steady state prebomb distributions, *J. Geophys. Res.*, this issue.

Veronis, G., The role of models in tracer studies, in *Numerical Models of the Ocean Circulation*, pp. 133–146, National Academy of Sciences, Washington, D. C., 1975.

Weiss, R. F., H. G. Ostlund, and H. Craig, Geochemical studies of the Weddell Sea, *Deep Sea Res., Part A*, *26*, 1093–1120, 1979.

Weiss, R. F., J. L. Bullister, R. H. Gammon, and M. J. Warner, Atmospheric chlorofluoromethanes in the deep equatorial Atlantic, *Nature*, *314*, 608–610, 1985.

K. Bryan, K. Dixon, and J. R. Toggweiler, Geophysical Fluid Dynamics Laboratory, NOAA, Princeton University, Princeton, NJ 08542.

(Received July 25, 1988;
revised January 20, 1989;
accepted February 9, 1989.)